

DUAL-MODE DUAL-BAND MICROSTRIP BANDPASS FILTER

LIM PAY SUN

**A project report submitted in partial fulfilment of the
requirements for the award of Bachelor of Engineering
(Hons.) Electronic Engineering**

**Faculty of Engineering and Science
Universiti Tunku Abdul Rahman**

May 2011

DECLARATION

I hereby declare that this project report is based on my original work except for citations and quotations which have been duly acknowledged. I also declare that it has not been previously and concurrently submitted for any other degree or award at UTAR or other institutions.

Signature : _____

Name : LIM PAY SUN

ID No. : 08UEB07420

Date : 23th May 2011

APPROVAL FOR SUBMISSION

I certify that this project report entitled **“DUAL-MODE DUAL-BAND MICROSTRIP BANDPASS FILTER”** was prepared by **LIM PAY SUN** has met the required standard for submission in partial fulfilment of the requirements for the award of Bachelor of Engineering (Hons.) Electronic Engineering at Universiti Tunku Abdul Rahman.

Approved by,

Signature : _____

Supervisor: Dr. Lim Eng Hock

Date : _____

The copyright of this report belongs to the author under the terms of the copyright Act 1987 as qualified by Intellectual Property Policy of University Tunku Abdul Rahman. Due acknowledgement shall always be made of the use of any material contained in, or derived from, this report.

© 2011, Lim Pay Sun. All right reserved.

Specially dedicated to
my beloved grandmother, mother and father

ACKNOWLEDGEMENTS

I would like to thank everyone who had contributed to the successful completion of this project. I would like to express my gratitude to my research supervisor, Dr. Lim Eng Hock for his invaluable advice, guidance and his enormous patience throughout the development of the research.

In addition, I would also like to express my gratitude to my loving parent and friends who had helped and given me encouragement. Furthermore, special thanks to UTAR OPAC system so that I can study the journals from the Institute of Electronic and Electrical Engineering (IEEE) database. Last but not least, I would like to thanks to the laboratory assistants that helped me in carry out whole project.

DUAL-MODE DUAL-BAND MICROSTRIP BANDPASS FILTER

ABSTRACT

Filters are essential in communication systems nowadays. They are usually used to select frequencies. Filters are playing an important role to select or confine the Radio Frequency (RF) signals within assigned spectral limits since the electromagnetic spectrum is limited by licensing issues and shared over different channels. A compact bandpass filter (BPF) using microstrip inter-digital microstrip lines are fabricated and printed on Duroid 6006 substrate. A 1.69/2.3GHz dual-mode dual-band microstrip BPF has been introduced. There are basically three major stages in this project, such as simulation, fabrication and experiment. In order to simulate the BPF performance with different configurations, a series of simulations based on HFSS version 8 will be used to run the simulation. A microstrip BPF will then be fabricated based on the HFSS version 8 simulated configurations and the filter response will be measured by using Vector Network Analyzer (VNA) in the laboratory. The measured results of the fabricated filters have good matching and reasonable agreement with the simulated results. After that, several case studies have been done on the proposed filter to study the relationship between different parameters. Lastly, discussions and recommendations have been proposed after the case studies. The proposed filter designs should be useful for compact transceiver modules.

TABLE OF CONTENTS

DECLARATION	ii
APPROVAL FOR SUBMISSION	iii
ACKNOWLEDGEMENTS	vi
ABSTRACT	vii
TABLE OF CONTENTS	viii
LIST OF TABLES	x
LIST OF FIGURES	xi
LIST OF SYMBOLS / ABBREVIATIONS	xiv
LIST OF APPENDICES	xv

CHAPTER

1	INTRODUCTION	1
	1.1 Background	1
	1.2 Aims and Objectives	2
	1.3 Project Motivation	3
2	LITERATURE REVIEW	4
	2.1 Microstrip Filter	4
	2.1.1 Microstrip Lines	6
	2.1.1.1 Dielectric Constant	8
	2.1.1.2 Effective Dielectric Constant	8
	2.1.1.3 Characteristic Impedance	9
	2.1.2 Microstrip Resonators	11
	2.1.2.2 Circular Patch Resonators	14

2.1.2.3	Triangular Patch Resonators	18
3	MICROSTRIP INTER-DIGITAL BANDPASS FILTER	23
3.1	Background	23
3.2	Research Methodology	24
3.2.1	Simulation Stage	24
3.2.2	Fabrication Stage	26
3.2.3	Experiment Stage	27
3.3	Proposed Filter Configurations	28
3.4	Results and Discussions	29
4	PARAMETER ANALYSIS	31
4.1	Case Studies	31
4.2	Gap	31
4.3	Width	31
5	CONCLUSION AND RECOMMENDATIONS	54
5.1	Conclusion	54
5.2	Recommendation	54
	REFERENCES	56
	APPENDICES	58

LIST OF TABLES

TABLE	TITLE	PAGE
--------------	--------------	-------------

LIST OF FIGURES

FIGURE	TITLE	PAGE
Figure 2.1:	Microstrip linkage	4
Figure 2.2:	Parallel-coupled microstrip line bandpass filter (BPF).	5
Figure 2.3:	Cross-slot microstrip rectangular patch resonating bandpass filter	5
Figure 2.4:	Three-pole microstrip semi-circular bandpass filter	6
Figure 2.5:	Cross-section view of microstrip	7
Figure 2.6:	Three single-mode patch resonators	12
Figure 2.7:	Transmission coefficients versus frequency for all the three resonator circuits	13
Figure 2.8:	Frequency response of the dual-mode rectangular patch resonators	14
Figure 2.9:	Microstrip-fed circular dual-mode filter with crossed slot and two triangular perturbation elements at the center	16
Figure 2.10:	Microstrip-fed circular patch with crossed and parallel slots	16
Figure 2.11:	Measured and simulated results for the filter of Fig. 2.9	16
Figure 2.12:	Measured and simulated results for the filter of Fig. 2.10	17
Figure 2.13:	Current distributions of the first two modes of a triangular microstrip resonator (a) Mode 1 (b) Mode 2	18

Figure 2.14: Stimulated resonant frequencies of the first two modes of triangular microstrip resonator	19
Figure 2.15: (a) Fabricated filter using triangular microstrip resonators operating at the mode 1; (b) Theoretical performance; (c) Experimental performance	20
Figure 2.16: (a) Fabricated filter using triangular microstrip resonators operating at the mode 2; (b) Theoretical performance; (c) Experimental performance	22
Figure 3.1: Top view of the dual-mode dual-band band pass filter	24
Figure 3.2: Rohde & Schwarz Tool Kit	28
Figure 3.3: Measured and stimulated S_{11} and S_{21} of dual-mode dual-band microstrip bandpass filter	29
Figure 4.1: Response of Case Studies I	32
Figure 4.2: The electric field when $g_1=0.021\text{mm}$	32
Figure 4.3: The electric field when $g_1=0.19\text{mm}$	33
Figure 4.4: Response of Case Study II	33
Figure 4.5: The electric field when $g_2= 0.075\text{mm}$	34
Figure 4.6: The electric field when $g_2= 0.055\text{mm}$	34
Figure 4.7: Response of Case study III	35
Figure 4.8: The electric field when $g_3=7.071\text{mm}$	36
Figure 4.9: The electric field when $g_3 = 7.069\text{mm}$	36
Figure 4.10: Response of Case Study IV	37
Figure 4.11: The electric field when $g_4=6.575\text{mm}$	38
Figure 4.12: Response of Case Study V	38
Figure 4.13: The electric field when $g_5=0.021\text{mm}$	39
Figure 4.14: Response of Case Study VI	40
Figure 4.15: The electric field when $g_6=0.075\text{mm}$	40
Figure 4.16: The electric field when $g_6=0.055\text{mm}$	41

Figure 4.17: Response of Case Study VII	42
Figure 4.18: The electric field when $W_2=0.10\text{mm}$	42
Figure 4.19: The electric field when $W_2=0.30\text{mm}$	43
Figure 4.20: Response of Case Study VIII	44
Figure 4.21: The electric field when $W_3=0.10\text{mm}$	44
Figure 4.22: The electric field when $W_3=0.30\text{mm}$	45
Figure 4.23: Response of Case Study VIII	46
Figure 4.24: The electric field when $W_4=1.10\text{mm}$	46
Figure 4.25: The electric field when $W_4=1.30\text{mm}$	47
Figure 4.26: Response of Case Study X	48
Figure 4.27: The electric field when $W_5=0.92\text{mm}$	48
Figure 4.28: The electric field when $W_5=0.94\text{mm}$	49
Figure 4.29: Response of Case study XI	50
Figure 4.30: The electric field when $W_6=0.89\text{mm}$	50
Figure 4.31: The electric field when $W_6=0.91\text{mm}$	51
Figure 4.32: Response of Case Study XII	52
Figure 4.33: The electric field when $W_7=1.40\text{mm}$	52
Figure 4.34: The electric field when $W_7=1.60\text{mm}$	53

LIST OF SYMBOLS / ABBREVIATIONS

c_p	specific heat capacity, J/(kg·K)
h	height, m
K_d	discharge coefficient
M	mass flow rate, kg/s
P	pressure, kPa
P_b	back pressure, kPa
R	mass flow rate ratio
T	temperature, K
v	specific volume, m ³
α	homogeneous void fraction
η	pressure ratio
ρ	density, kg/m ³
ω	compressible flow parameter
ID	inner diameter, m
MAP	maximum allowable pressure, kPa
MAWP	maximum allowable working pressure, kPa
OD	outer diameter, m
RV	relief valve

LIST OF APPENDICES

APPENDIX	TITLE	PAGE
APPENDIX A:	Journals	58

CHAPTER 1

INTRODUCTION

1.1 Background

Bandpass filter is an electrical design component that allows signal to pass through a desired frequency range and rejects other unwanted frequencies outside the desired range. The rapid growth of mobile and wireless communication system technology in today's world has increased the need of applying the microstrip bandpass filters into design. Many of these communication systems are complex and will require the circuitry design to be small in size, low cost, easy to fabricate, high performance and multi-frequency. From IEEE Xplore, there are more than 600 microstrip filter publications in recent 10 years, and these publications continue to increase more and more, this shows a positive and strong growth of research in these areas.

There are many type of filter designs and patterns, which designed based on different characteristics such as Butterworth, Cherbysev and Elliptic filters, or bandwidth property such as wideband or dualmode properties. Dual-band filter is mainly used to allow two different signals to go through within two frequency ranges at the same time rather than common single frequency range filter. Wideband bandpass filter can be used in application that passes wide range of frequencies in a single spectrum. For instance, microstrip filters have been extensively applied to modern radio frequency and microwave system. Thus, filter size is one of the concerns in the filter design. The filter is design to ensure that it can fit into the

electronic devices. Besides, the losses of the filter are playing an important role because they will affect the performance of the filters.

1.2 Aims and Objectives

This project studies the property of the microstrip bandpass filter and to design a dual-mode dual-band microstrip bandpass filter by using HFSS simulation software. This objective helps to gain fundamental knowledge in microstrip filter. There are a lot of journals and articles which can be explored through IEEE Xplore database under the Universiti Tunku Abdul Rahman (UTAR) OPAC system.

The project aims to design a microstrip bandpass filter which is simple and easy to fabricate. The designed filter must be a dual-band and dual-mode bandpass device that resonates in the frequency range of 1 to 5 GHz. Microstrip filter can be designed using a lot of inter-digital microstrip lines. There is no limitation on the substrates being used as well.

On the other hand, this project aims to design an inter-digital microstrip bandpass filter with dual mode property. From the study, there are less number of filters that being designed using inter-digital microstrip lines. Hence the project is aiming at designing the world's first dual-mode dual-band bandpass microstrip inter-digital filter using the HFSS software. Simplicity and small size are among the major concerns of the inter-digital features as well. The filter will be unique, simple, and high-performing.

Through this project, students will have a better understanding of the microstrip bandpass filter properties. Besides, students are able to design filters by using the HFSS software. Furthermore, students will be able to measure the filter responses by using Vector Network Analyzer and compare the measured result with the simulated one. Based on the results, students will able to do an analysis of the results and troubleshoot if any problem exists.

1.3 Project Motivation

The project motivation is to design the microstrip bandpass filters that are publishable in the IEEE Xplore journals. After completing the literature review throughout the journals in IEEE Xplore, knowledge in filter design has widened. However, some of the resonating filters are very complex and not applicable to commercial products. This can incur high fabrication cost. Therefore, the goal of this project is to design a simple, high-performing, and small-size microstrip bandpass filter that has results comparable to those published in IEEE Xplore.

CHAPTER 2

LITERATURE REVIEW

2.1 Microstrip Filter

In modern wireless and mobile communication systems, Radio Frequency (RF) and microwave filter are important and essential components. No doubt, filters are playing an important role in the RF and microwave applications. Filters with smaller size, lighter weight, higher performance, and lower insertion loss are of high demand. Microstrip filters can fulfil the requirements stated above. Besides wireless and mobile communication systems, low-temperature cofired ceramics (LTCC), high-temperature superconductor (HTS), monolithic microwave integrated circuits (MMIC), microelectromechanic system (MEMS) and micromachining technology, have driven the rapid development of the new microstrip filter than other microwave and RF filters. Figure 2.1 shows the microstrip filters linkage.

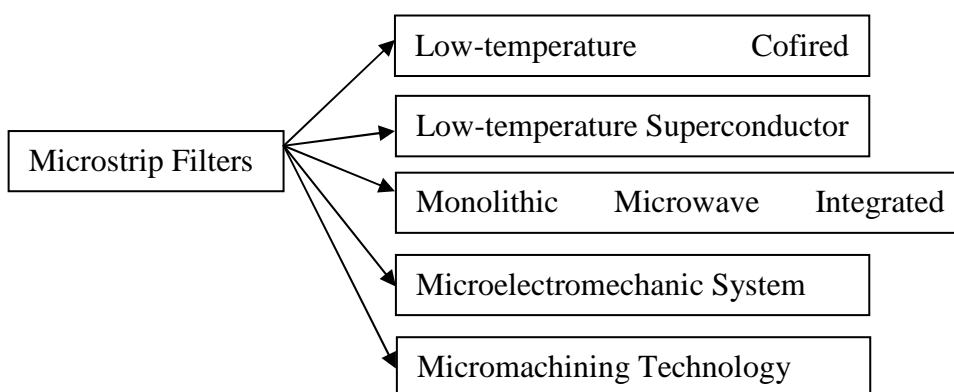


Figure 2.1: Microstrip linkage

Microstrip filters can be designed in various patterns depending on different requirements. Each microstrip filter consists of its individual properties and characteristics. The common microstrip designs that available in market are such as rectangular patch filter, circular patch filter, triangular patch filter and etc. The figures below show some of the microstrip filters that were published in the IEEE papers. Further discussions on the filter will be included in Chapter 2.2 onwards.

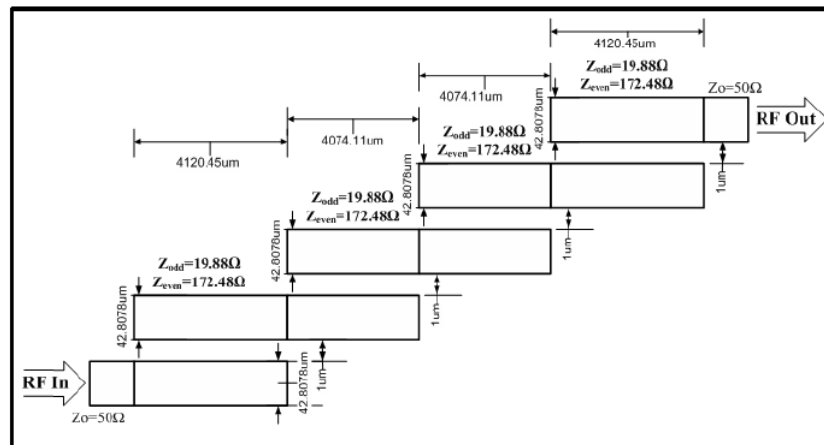


Figure 2.2: Parallel-coupled microstrip line bandpass filter (BPF).

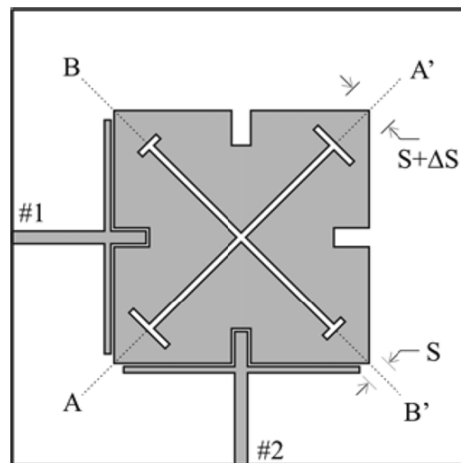


Figure 2.3: Cross-slot microstrip rectangular patch resonating bandpass filter

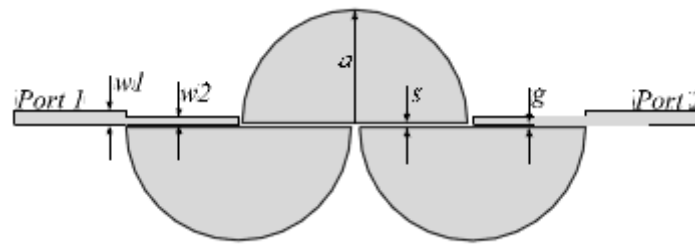


Figure 2.4: Three-pole microstrip semi-circular bandpass filter

By using the computer-aided design (CAD) tools, the process of designing the microstrip bandpass filter will be easier and consumes less time as designers are able to simulate the design performance upfront and perform fine-tuning on the design based on the simulated results before proceeding any fabrication. The increase in computer processing power fastens the development of CAD simulation tools. In return, this helps designers to design filter products that will lower the cost of building prototype samples, including tooling, material and labor resource. CAD tools provide precise design with less iteration and design resource costs include those for design, tuning, fabrication and testing can be minimized. Thus, in this project, a powerful HFSS tool has been selected and will be used in this project as the microstrip bandpass filter design CAD tools. The HFSS tools always produce a simulated result that comparable to measured result.

2.1.1 Microstrip Lines

Microstrip is a planar transmission line that basically consists of a thin-film strip in intimate contact with one side of a flat dielectric substrate, with a similar thin-film ground-plane conductor on the other side of the substrate. It is similar to stripline and coplanar waveguide, and it is possible to integrate all three on the same substrate. According to Encyclopedia, microstrip was developed by ITT laboratories by Grieg and Engelmann in December 1952 as a competitor to stripline. According to Pozar, the early microstrip work used fat substrates, which allowed non-TEM

waves to propagate which makes results unpredictable. In the 1960s the thin version of microstrip started became popular.

Microstrip can be fabricated using printed circuit board (PCB) technology and is used to convey microwave frequency signals. It consist of a conducting strip separate from a ground plane by a dielectric layer which known as substrate. Figure 2.5 shows a cross section view of a microstrip. A is representing conductor which are separate from ground plane (D) by dielectric (C). And the upper dielectric (B) is typically air.

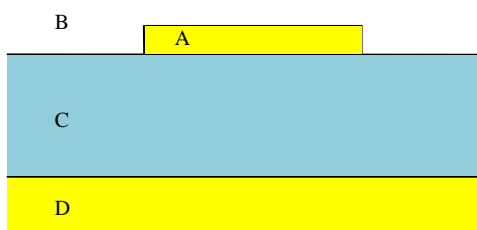


Figure 2.5: Cross-section view of microstrip

Microstrip can be used to design antennas, couplers, filters, power dividers and etc. The material costs are lower than the traditional waveguides since the entire microstrip is just a patterned metal and a ground plane only, and it also much lighter and more compact than the waveguides. Since microstrip is not enclosed as a waveguide, it is susceptible to crosstalk and unintentional radiation. Unlike stripline, microstrip can mount all the active components on top of the board. However, the disadvantages are that microstrip generally has lower power handling capacity and higher losses. External shield may be needed for circuits that require higher isolation such as switches.

In this project, microstrip has been chosen for the filter design because it is a proven technology and the shielding problem can be solved easily by encapsulating the filter in a metallic box. Besides, crosstalk and unintentional radiation are not an issue in this project as well. Furthermore, plenty of microstrip filters design can be found in the IEEE Xplore database. References are easy to find for microstrip filter.

2.1.1.1 Dielectric Constant

Microstrip can be fabricated on different substrates based on the requirement of the design. For a lower cost, microstrip devices can be built on the ordinary Duroid 6006 substrate. Dielectric constant is a measure of the extent to which it concentrates electrostatic lines of flux. For example, FR-4 has a dielectric constant of 4.4 and R6006 duroid has 6.15 at frequency of 10 GHz. And by definition, the dielectric constant of vacuum is equal to 1. Dielectric constant is frequency dependent.

In this project, Rogers Duroid 6006 has been chosen as the substrate for the microstrip bandpass filter design. The substrate is expensive because it is relatively thin and high in dielectric constant. It is not available in the Malaysia and has to be ordered from United States.

2.1.1.2 Effective Dielectric Constant

Electromagnetic wave carried by a microstrip line exists partly in the dielectric substrate, and partly in the air above it (as shown in Figure 2.5). In general, the dielectric constant of the substrate will be different (and greater) than air, so the wave is travelling in an inhomogeneous medium. In consequence, the propagation velocity is somewhere between the speed of radio waves in the substrate, and the speed of radio waves in air. This behaviour is commonly described by stating the effective dielectric constant of the microstrip. Effective dielectric constant is an equivalent dielectric constant of an equivalent homogeneous medium. As part of the fields from the microstrip conductor exists in air, the effective dielectric constant is less than the substrate's dielectric constant.

According to Constantine A. Balanis, the effective dielectric constant can be calculated by using formulas below where W represents width of strip, H represents height of the substrate and ϵ_r represents dielectric constant of substrate. Note that there are different solutions for cases where $W/H < 1$ and $W/H > 1$.

$$\begin{aligned}
 & \text{when } \left(\frac{W}{H}\right) < 1 \\
 & \epsilon_e = \frac{\epsilon_r + 1}{2} + \frac{\epsilon_r - 1}{2} \left[\left(1 + 12\left(\frac{H}{W}\right)\right)^{-1/2} + 0.04\left(1 - \left(\frac{W}{H}\right)\right)^2 \right] \\
 & \text{when } \left(\frac{W}{H}\right) \geq 1 \\
 & \epsilon_e = \frac{\epsilon_r + 1}{2} + \frac{\epsilon_r - 1}{2} \left(1 + 12\left(\frac{H}{W}\right)\right)^{-1/2}
 \end{aligned} \tag{2.1}$$

In this project, HFSS version 8 has taken effective dielectric constant into account during simulation process. Hence all the calculations have been done using the simulation software and hence there should not be an issue for this project. This is one of the advantages using CAD simulation software.

2.1.1.3 Characteristic Impedance

The characteristic impedance Z_0 is important in microstrip lines design, it will affect the reflection loss S_{11} . The reflection loss is related to the characteristic impedance and also load impedance by formula, $S_{11} = \frac{Z_{in} - Z_0}{Z_{in} + Z_0}$. In order to minimize the reflection loss at the input port, the characteristic impedance of microstrip must be equal to the input of the impedance. In this project, the Vector Network Analyzer (VNA) connector input impedance will be the input impedance. Most of the input ports are designed at 50ohm, so as the VNA connector input impedance. Therefore, the microstrip lines should be designed to achieve 50ohm to prevent any reflections.

The characteristic impedance is also a function of height (H) and width (W) of microstrip lines. Note that effective dielectric constant value is required for the microstrip characteristic impedance calculation. According to Bahl and Trivedi[1], the characteristic impedance of microstrip lines can be calculated by using formulas below.

$$\begin{aligned}
 & \text{when } \left(\frac{W}{H}\right) < 1 \\
 & Z_0 = \frac{60}{\sqrt{\epsilon_{eff}}} \ln\left(8 \frac{H}{W} + 0.25 \frac{W}{H}\right) \text{ (ohms)} \\
 & \text{when } \left(\frac{W}{H}\right) \geq 1 \\
 & Z_0 = \frac{120 \pi}{\sqrt{\epsilon_{eff}} \times \left[\frac{W}{H} + 1.393 + \frac{2}{3} \ln\left(\frac{W}{H} + 1.444\right)\right]} \text{ (ohms)}
 \end{aligned} \tag{2.2}$$

The very first step in this project is to design the microstrip lines that can achieve 50ohm of characteristic impedance. From the formulas above, there are three variables in the calculation which are ϵ_{eff} , Width(W) and Height(H). Since ϵ_{eff} and height is constant for the substrate, the only variable is the width of the microstrip line.

Since the formula is quite complicated, writer has to substitute different W value in order to get 50ohm characteristic impedance. At first, writer has to verify the ratio of W/H and determine which formula to be used. It is time consuming for the calculation on different substrate. Fortunately, some of the web application and software are able to calculate the width of the microstrip lines by entering the desire characteristic impedance, height of the substrate and dielectric constant of the substrate. Then the software will performs the calculation within seconds and shows the value. It has simplified the microstrip lines design work and most importantly consume less time. For instance, one of the useful software writer used for characteristic impedance calculation in this project is TX Line 2003. The software is

easy to control and writer able to get the width value easily by key in height of the substrate, thickness of the strip, and dielectric constant of the substrate. The microstrip width calculation will be cover in Methodology part.

2.1.2 Microstrip Resonators

Microstrip resonators can be designed in various patterns as shown in Figure 2.1-2.4. Before designing the microstrip band pass filter, write has to do some literature studies through IEEE Xplore about the microstrip resonators. Besides, it is also to ensure that the effort spent in design has not been researched by others nor published in the IEEE Xplore before. The author has selected three common types of resonators to be discussed in the following chapters. The types of resonators that covered are rectangular patch resonators, circular patch resonators and triangular patch resonators.

2.1.2.1 Rectangular Patch Resonators

In order to increase the power handling capability, several types of microstrip patch resonators including square and circular patches have been used for the filter designs. An associated advantage of microstrip patch resonators is their lower conductor losses as compared with narrow microstrip line resonators. Although a patch resonator normally has a larger size, this would not be a problem for the applications in which the power handling or low loss has a higher priority. Particularly, the size may not be an issue at all for the micro-machined filters that operate at very high frequencies.

From the paper of Lei Zhu, Boon Chai Tan, and Siang Juay Quek, a cross-slotted patch resonator is developed, the simultaneous size and loss reduction, and dual-mode bandpass patch filter is built by suitably selecting the unequal cross-slot lengths along the two orthogonally diagonal planes. (as shown in Figure 2.3).

A comparative study is first carried out to exhibit the resonant frequency versus cross-slot dimensions, targeting the construction of a miniaturized patch resonator. A dual-mode filter is then designed with suitable adjustment of the two unequal T-shape stub lengths. The resonance behaviors of the three single-mode patch resonators with the sketches showed in Fig. 2.6, namely, resonators (A) to (C), respectively. By etching the four slits at the center of four sides of a square patch and entering the two feeding lines into the slits, the patch resonator (A) is formed to facilitate the feeder-to-resonator coupling enhancement in addition to slight reduction of resonant frequency. A pair of crossed slots is then etched on the slit-loaded patch (A) so as to make up a star-type cross-slotted patch resonator (B). Such the paired crossed-slots bring out an additional inductance, thus reducing the resonant frequency and radiation loss. By terminating the crossed slots at the ends with the T-shape slot stubs, the resonator (C) is built up as sketched in Fig. 2.6.

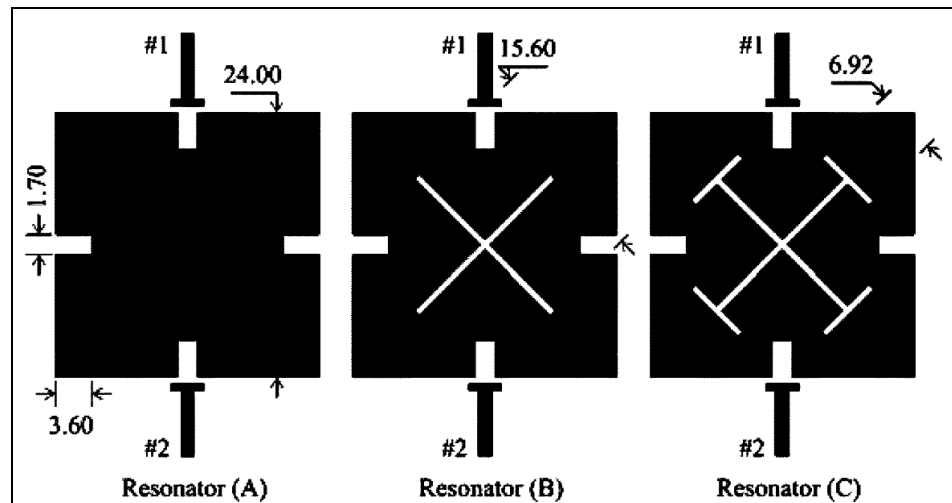


Figure 2.6: Three single-mode patch resonators

In this study, the above three patch resonators are formed on the substrate of Taconic FR4 with the parameters of $\epsilon_r = 4.2$, $h = 1.6\text{mm}$, and $\tan \Delta = 0.016$, and their relevant frequency responses are numerically simulated via Agilent Momentum software.

With the T-shape slot stubs installed at each end of the cross slots, the current densities flowing in opposite directions are better cancelled and the radiation area of this patch is electrically reduced. As a result, the proposed inductively loaded cross-slotted patch resonator (C) besides lower the resonant frequency or miniaturize the resonator size under the unchanged frequency but also reduce the concerned radiation loss to a great extent.

From Fig. 2.7, it showed the transmission coefficients versus frequency for all the three resonator circuits. As opposed to 2.95 GHz of a normal square patch resonator with the side length of 24.0 mm, the resonant frequency of its corresponding slit-loaded patch resonator (A) is slightly lowered to 2.81 GHz. As the crossed slots with the length of 15.6 mm are centrally loaded on the slit-loaded square patch, the resonant frequency of the resonator (B) is largely reduced to 2.45 GHz. Its value is observed to be further decreased to 2.07 GHz as the T-shape slot stubs are introduced in the resonator (C) in Fig. 2.6.

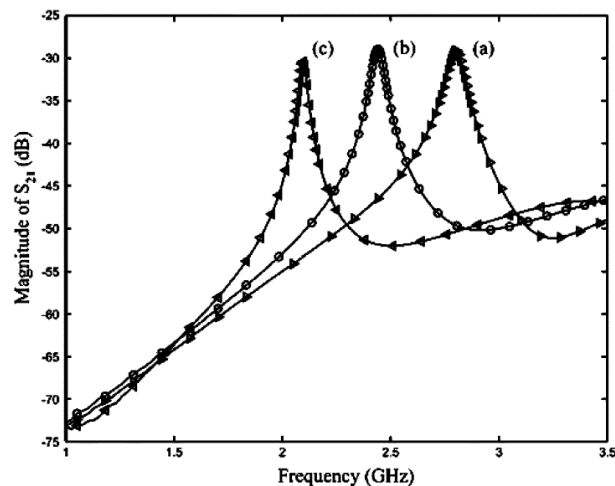


Figure 2.7: Transmission coefficients versus frequency for all the three resonator circuits

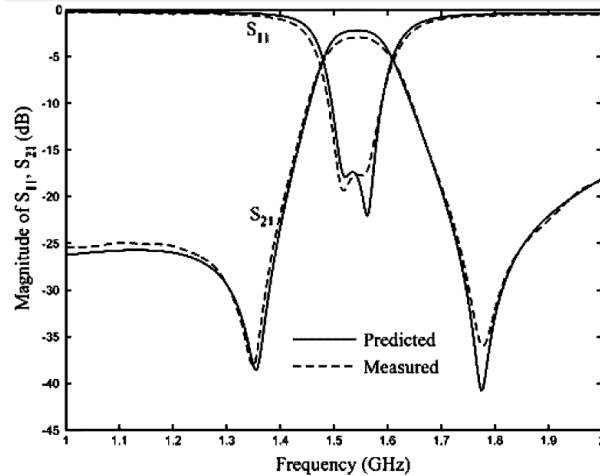


Figure 2.8: Frequency response of the dual-mode rectangular patch resonators

After study this journal, the T-shape slot stubs studies have been carried out. It is important as it established the miniaturized dual-mode patch resonator bandpass filter with the unequal T-shape slot stubs at the ends. Moreover, comparative investigation is implemented to demonstrate several attractive features of the inductively loaded cross-slotted patch resonator developed here, such as size and radiation loss reduction.

2.1.2.2 Circular Patch Resonators

From the journal paper of Yatendra Kumar Singh and Ajay Chakrabarty, dual-mode circular patch bandpass filters has been miniaturized with wide harmonic separation. This letter presents miniaturization of a circular patch by modifying it with a properly oriented crossed slot, which increases the path length of the fundamental current but keeps the second harmonic current path length unaltered. This brings down the resonance frequency of the fundamental mode and keeps the location of the next higher order mode unchanged, effectively increasing the separation between the two fundamental modes.

Similarly, a comparative study is first carried out to exhibit the resonant frequency versus cross-slot dimensions. In this study, a circular patch resonator is

designed at 2.355 GHz. The radius of the patch comes out to be 18.0 mm. The patch, when simulated using IE3D on an FR4 substrate of relative permittivity 4.3, loss tangent 0.01, and thickness 1.5875 mm, resonates at 2.2825 GHz, which is quite close to the designed resonance frequency.

To reduce the resonance frequency of the fundamental mode, the length of the path taken by the current from one port to the other has to be increased. This can be done by introducing obstacles for the fundamental current on the patch by creating rectangular slots or circular holes. In general, an obstacle increases the path length of the second order mode current also, reducing the harmonic separation between the fundamental and the second resonances.

If two orthogonal slots are created on the circular patch and oriented as shown in Fig. 2.9, the fundamental mode frequency will drop because of increase in its current path length. The second higher order mode frequency, however, will remain almost unaffected as the slots are parallel to the currents and do not alter their path.

The journal has shown about a study on coupling structure as well. Two triangular cuts at the center have been used to introduce coupling between the two orthogonal degenerate TM modes of the patch. The proposed perturbation technique gives rise to two attenuation poles on both sides of the passband. The poles do not appear if the conventional perturbation technique of putting one cut at the periphery is used. They also do not appear if the perturbation cuts are made in the first and the third quadrant of the patch instead of the second and the fourth. Fig. 2.4 shows the final configuration of the filter.

Besides, the journal has also shown additional slots that can be created parallel to the crossed slot arms. (as shown in Fig. 2.9). The resultant configuration further increases the current path of the fundamental mode. Two triangular cuts connected by a slot have been used as perturbation element. The dual-mode resonator designed using this configuration is highly miniaturized and has much better harmonic separation. The final configuration is shown in Fig. 2.9. All simulations in

this paper were carried out using IE3D software. All slots have the same width of 0.5 mm and the two triangular perturbations are identical right-angled isosceles triangles.

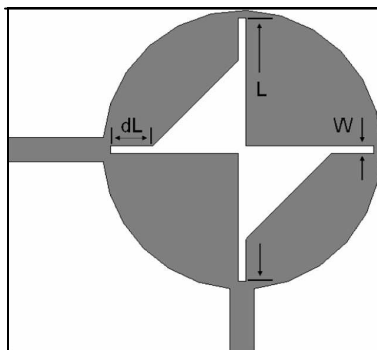


Figure 2.9: Microstrip-fed circular dual-mode filter with crossed slot and two triangular perturbation elements at the center

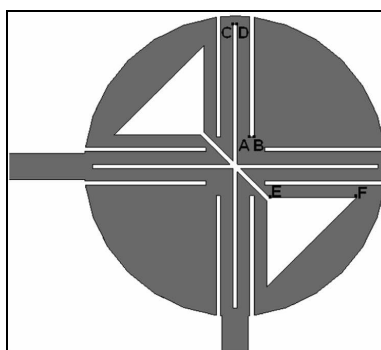


Figure 2.10: Microstrip-fed circular patch with crossed and parallel slots

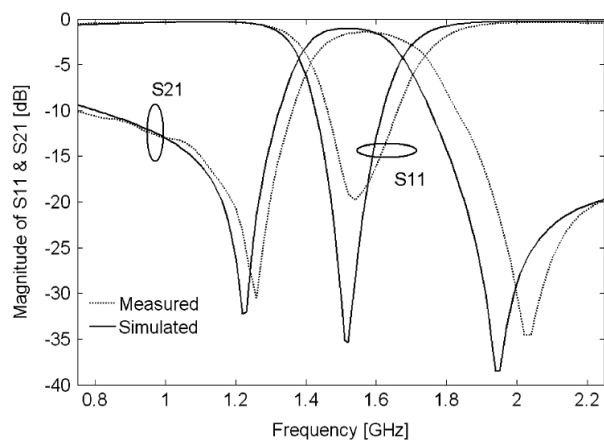


Figure 2.11: Measured and simulated results for the filter of Fig. 2.9

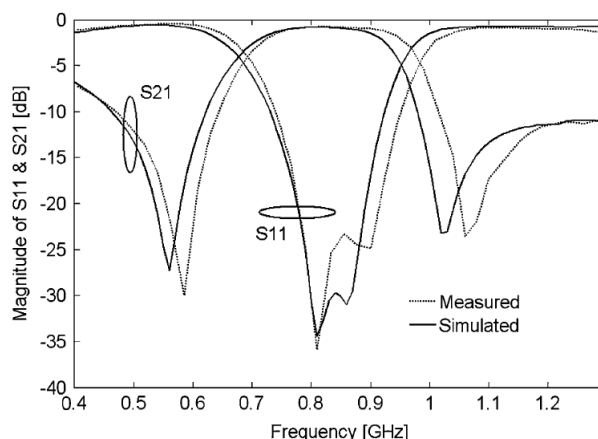


Figure 2.12: Measured and simulate results for the filter of Fig. 2.10

The simulated and measured results for the first filter (Fig. 2.9) are shown in Fig. 2.11. The fabricated filter gives 57.77% reduction in size compared to a circular patch resonator. Fig. 2.12 shows the measured and simulated results of the second filter (Fig. 2.10). From the measured data, it is found that this filter is smaller by 87.40% compared to a circular patch resonator. The insertion loss of the two filters in the passband was mainly affected by substrate loss.

As the journal has shown, it uses a different approach to design a circular patch resonator compare to rectangular ring resonator. First, the radius of circular patch resonator will be determining the resonant frequency of the resonator. However, it is still depending on which dominant mode is considered. In this journal, TM_{110} has been considered during the circular patch resonator design. Besides, the coupling coefficient is affected the gap between the circular resonators.

As a conclusion, circular resonator is easy to design but the signal coupling would be much harder to optimize than rectangular ring resonators due to its shapes. Since the shape of circular resonator is round, it is hard to design a feeder. A curl shape feeder must be designed. The curl shape feeder is having two major drawbacks. Firstly, it is hard to maintain the gap distance to be constant for curl shape feeder. Secondly, it is hard to draw and fabricate compare to the rectangular straight feeder.

2.1.2.3 Triangular Patch Resonators

From the paper of Jia-Sheng Hong and Michael J. Lancaster, “Microstrip Triangular Patch Resonator Filter” has been designed on 0.635mm RT/Duroid substrate with a relative dielectric constant of 10.8 and thickness of 12.7mm. The designs were done using the full-wave EM simulator. This journal has designed and fabricated two three-pole microstrip triangular resonator bandpass filters.

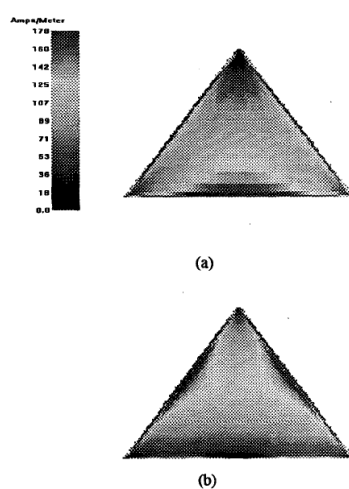


Figure 2.13: Current distributions of the first two modes of a triangular microstrip resonator (a) Mode 1 (b) Mode 2

Fig. 2.13 showed the field distributions of two distinguishable resonant modes of a microstrip triangular patch resonator, which were obtained using a full-wave electromagnetic (EM) simulator. It can clearly be identified that the mode 1 in Fig. 2.13(a) has almost current concentrated on the base, whereas the mode 2 in Fig. 2.13(b) has almost current on the both slant sides. It is these two modes that will be operated in filters to result in different filtering characteristics.

Fig. 2.14 plot some simulated results of the resonant frequencies as a function of the vertical height b for a given base length a . f_{01} is the resonant frequency of mode 1, while f_{02} is the resonant frequency of mode 2. As can be seen f_{01} , the resonant frequency of mode 1 is less dependent on b . This may be understood

because this mode is mainly based on the base of the triangle as shown in Fig.2.13 (a). Obviously, one can use this property to control the separation of the two modes. When $b=13\text{mm}$ in Fig.2.14, the isosceles triangle degenerates to an equilateral triangle, and the two modes have the same resonant frequencies.

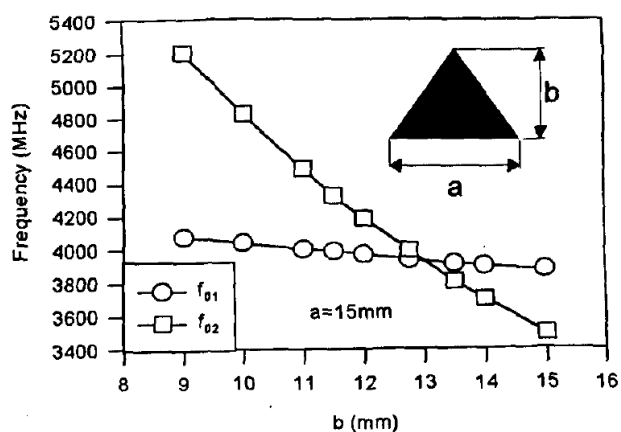
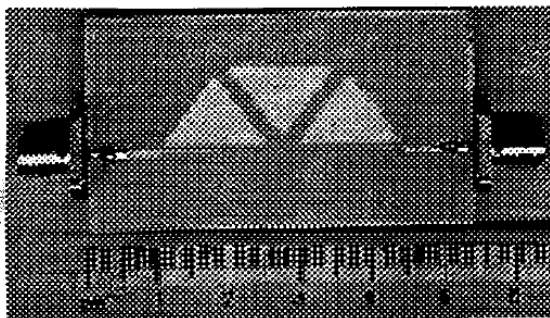
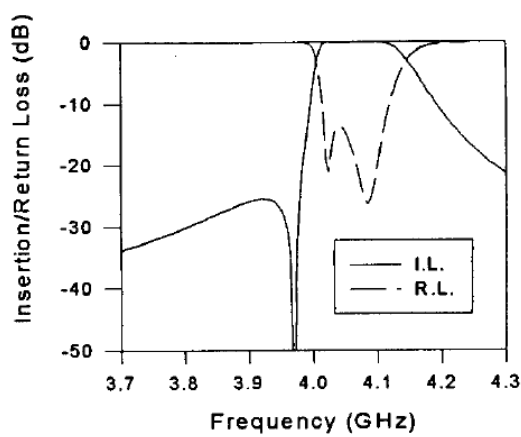


Figure 2.14: Stimulated resonant frequencies of the first two modes of triangular microstrip resonator

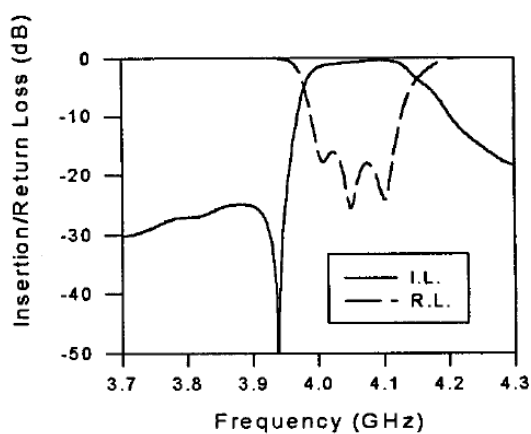
Fig. 2.15 (a) shows the fabricated filter that was designed to operate at the resonant mode 1 of Fig. 2.13(a) and to have an asymmetric response with a finite-transmission zero on the low stopband. The full-wave EM simulated performance of the filter is plotted in Fig. 2.15 (b), while the measured one in Fig. 2.15 (c).



(a)



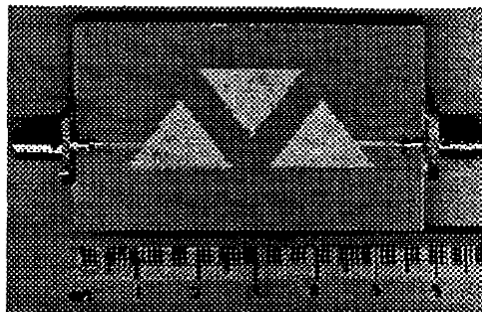
(b)



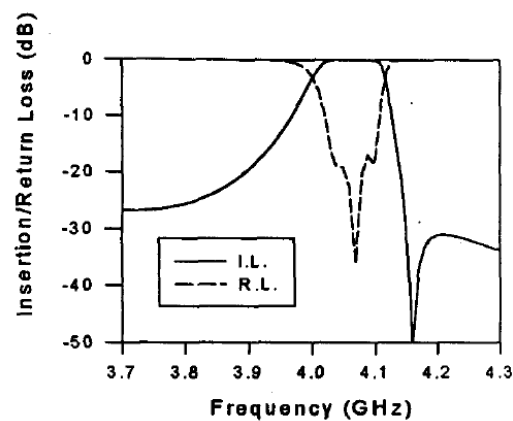
(c)

Figure 2.15: (a) Fabricated filter using triangular microstrip resonators operating at the mode 1; (b) Theoretical performance; (c) Experimental performance

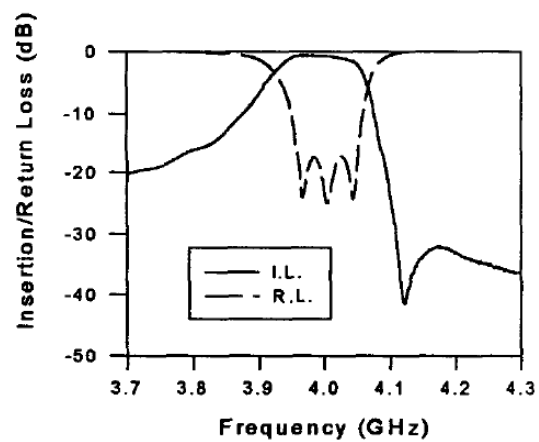
The filter that was designed to operate at the mode 2 of Fig. 2.13 (b) and to have a finite frequency transmission zero located on the high stopband is illustrated in Fig. 2.16 (a). It should be noticed that despite of a similarity of the cascaded resonator structure with Fig. 2.15 (a), the input and output coupling structures and locations in the two filters are different because they operate at different modes. The full-wave EM simulated performance of the filter is plotted in Fig. 2.16 (b), while the measured one in Fig.2.16 (c), where the finite-transmission zero as compared with the previous filter is located on the other side of the passband, improving the selectivity on that side as what is desired.



(a)



(b)



(c)

Figure 2.16: (a) Fabricated filter using triangular microstrip resonators operating at the mode 2; (b) Theoretical performance; (c) Experimental performance

In this journal, the author has performed study on the different approach for triangular patch resonator to have transmission zeros. The author demonstrated that microstrip triangular patch resonator filters could have some advanced filtering characteristics in a simple circuit topology of cascading resonators.

CHAPTER 3

MICROSTRIP INTER-DIGITAL BANDPASS FILTER

3.1 Background

Since there are increasing demands for designing compact, high performance and high selectivity dual-mode and dual-band filters for modem mobile and wireless communications systems application. It is commonly seen that planar filter which can be fabricated using printed circuit technologies would be preferred whenever it is available and will be suitable because of its smaller size and lower fabrication cost. Therefore, there has been a growing interest in developing new planar filter structures. The rapid progress in mobile and wireless communication technology has increased the need of dual-bandpass filter.

However, there are only few studies on dual-band filters realized by dual-mode resonators. Thus, an idea to develop a dual-mode dual-band microstrip bandpass filter has been come out in order to fulfil the high demand in market. The design of the dual-mode dual-band microstrip bandpass filter is shown in Figure 3.1. The bandpass filter has been design by using inter-digital microstrip lines by suitably selecting the unequal lengths and widths.

The dimension of the band pass filter that been designed is $40 \times 30 \text{ mm}^2$ ($l_1 \times W_1 \text{ mm}^2$). It is fabricated on Ruroid 6006 with thickness of 0.635mm and dielectric constant of 6.15. The dimension details of the configuration and results will be discussed later in the following Chapter 3.3. The result of the filter was measured with a Vector Network Analyze.

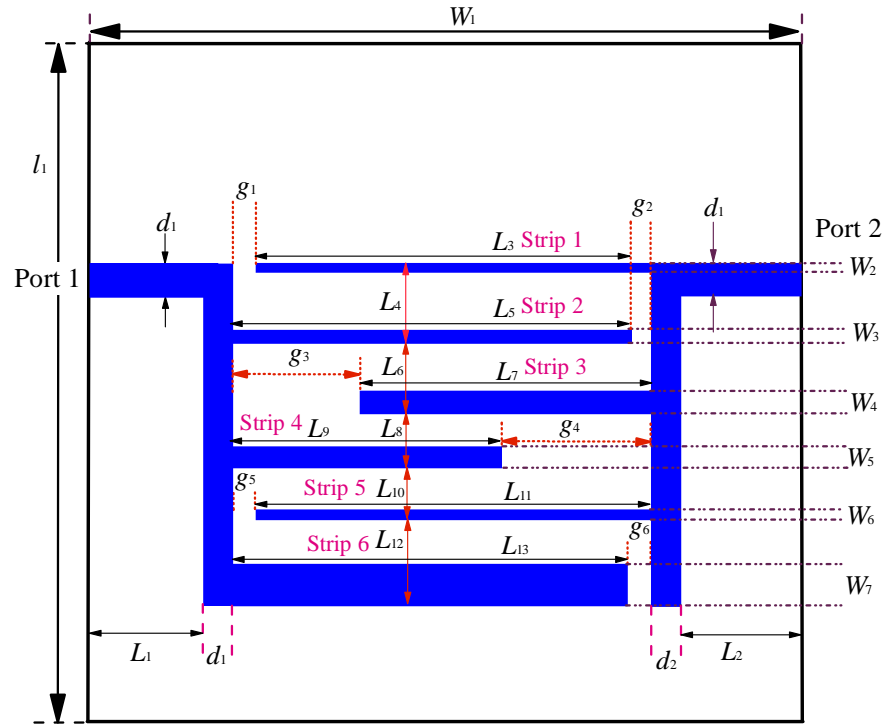


Figure 3.1: Top view of the dual-mode dual-band band pass filter

3.2 Research Methodology

Generally, there are three main stages in this project, which are simulation stage, fabrication stage and experiment stage. In this chapter, the filter design procedure will be discussed from simulation until experiment stage.

3.2.1 Simulation Stage

After exploring the journals in IEEE Xplore and did some literature review on dual-mode dual-band microstrip bandpass filters, a simulation based on few journals have been simulated on HFSS version 8. The result obtained is quite similar to the simulation shown in the journals. However, the simulated result did show some

different and it might be due to different simulation software being used. After getting consult from supervisor, the simulation result generated by HFSS version 8 is acceptable, HFSS has been chosen as our simulation software for this project.

HFSS is chosen as the simulation software to be used in this project, few tutorials have been gone through to ensure writer familiar with the software and hand-on experience on features consist in the software first before modeling design using the simulation tool. HFSS contains tutorials for new beginner. It is meant for beginner to understand and hand-on with all the features, it took writer around a week to complete the tutorials.

Then, a 50 ohm of characteristic impedance feed line has been formed in order to avoid any reflection of the signal goes in. The characteristic impedance of feed line can be calculated by using Equation 2.2 or software such as TX Line 2003. In this project TX Line 2003 has been used due to simplicity and accuracy of the software. According to TX Line 2003, the width of a 50 ohm feed line on a Duroid 6006 substrate with dielectric constant of 6.15 and thickness of 0.635 mm is 0.93 mm.

Later on, few testing have been carried out on the microstrip inter-digital bandpass filter. Plenty of simulations have been generated and most of them are not working well. At first, the filter has been simulated with different widths and lengths. Then different gap distances have been tried for each capacitive coupling position. At the end, a final version of microstrip inter-digital bandpass filter configuration has been proposed as in Figure 3.1.

Dual-mode filter is more preferred compare to single-mode filter nowadays. As studies shown in Zhu Lei papers, perturbation elements can be introduced by adding crossed-slot into rectangular patch which excites dual degeneration modes. Besides crossed-slot, other configurations may be used in this case. In this project, inter-digital microstrip lines have been used. It consumes some time to run the simulation during the process of designing the filter. A simulation may goes up to half an hour depends on complexity of the design. However, while waiting the simulation result, writer did some analysis on previous results. Writer looked into the

potential improvement that can be made by analyzing the previous results and this has spent around two months on this stage.

3.2.2 Fabrication Stage

Next, will be the fabrication stage. The simulation results have been sent to supervisor to verify before fabrication process. Substrate Duroid 6006 that used in this filter design is available on the market. The Duroid 6006 used in this project is with single-sided, photo print and UV positive photoresist properties. During fabrication, the filter designs have to be printed on tracing paper first before printed on the board. The size of filter must be 100% exact size of the simulation filter design as the gap for capacitive coupling is extremely sensitive. A 0.01mm mismatch may affect the final result. Hence writer has used several approaches in order to print exact filter design layout on tracing papers. At first, writer has asked some PCB maker in industrial line to fabricate the board for us. Industrial PCB maker has the advance equipment that can help them achieve 0.01 mm accuracy or even more.

However, due to cost and time constraint, writer had to fabricate the board herself. EAGLE CadSoft was used to draw the filter before print on the tracing paper. At first, an exact size filter layout has been drawn by using EAGLE CadSoft and printed on tracing paper. After the first board came out, writer found that the gap is too large compare to design layout. After discussed with supervisor, writer found that it may due to light dispersion properties. During fabrication, the Duroid 6006 is printed by photo printing. The tracing paper located on top of the board. As the UV light exposed to the gap, UV light will disperse and make the gap larger than 0.1 mm. To prevent this occurs, writer had reduce the gap to 0.8 mm in EAGLE CadSoft and the problem has been solved. According to supervisor, the rule of thumb is by reducing 20% of actual size in design.

3.2.3 Experiment Stage

Experiment is the last stage in the verification after fabrication. Since prototype has been fabricated, it will then be measured and to compare with simulation results. The equipment used for this experiment is Rohde & Schwarz ZVB8 Vector Network Analyzer (VNA). The frequency range of the equipment is 300 kHz to 8 GHz. The filter designs are not more than 6 GHz, hence the equipment is still applicable to the experiment.

Before experiment, writer had to do calibration on the VNA because imperfections exist in even the finest test equipment and, if uncorrected, these imperfections will cause the equipment to yield less than ideal measurements. The basis of network analyzer error correction is the measurement of known electrical standards, such as a thru, open circuit, short circuit, and precision load impedance. By calibrating the network analyzer with these standards, only then it can compensate for its inherent imperfections. With such, the connector and cable are the main component that writer need to calibrate the difference phase of signal induced due to matching. Through calibration, the VNA only then able to self adjust on the S-parameters after the calibration process. The calibration process required to connect two ports of VNA to five different port of tool kit. Tool kit has five ports in total, three for single-port (Open, Short, and Match) and two for two-port (Thru). The experiment can then be started after the calibration process. The filter 2 ports were then connected to each of the VNA port respectively. Frequency range and sweep point had to be set in order to similar to simulation result. The experiment results have been recorded and further discussed in following chapters.



Figure 3.2: Rohde & Schwarz Tool Kit

3.3 Proposed Filter Configurations

A dual-mode dual-band microstrip bandpass filter initial design pattern had been defined. The microstrip bandpass filter is formed by coupling few microstrip lines as show in Figure 3.1. A Duroid 6006 substrate of $\epsilon_r = 6.15$ and thickness $h = 0.635\text{mm}$ was used in the microstrip bandpass filter design here.

The feed line has a width of $d_1 = 0.93\text{mm}$ and a length of $L_1 = 5\text{mm}$. The feed line is couple efficiency to a vertical strip line, thus the vertical strip line has a width of $d_1 = 0.93\text{mm}$ on the left-hand side, $d_2 = 0.935\text{mm}$ on the right-hand side, and a total length of the vertical strip line is 10.2mm ($L_4 + L_5 + L_6 + L_7 + L_8 + L_9$). The first, third and the fifth strip lines are connected to the right-hand side of the vertical line. The dimensions of the first, third and fifth strip lines are given by $L_3 = 18.115\text{mm}$, $W_2 = 0.20\text{mm}$, $L_7 = 11.065\text{mm}$, $W_4 = 1.20\text{mm}$, $L_{10} = 18.115\text{mm}$, $W_6 = 0.90\text{mm}$. For the second, fourth and sixth strip lines were designed in different parameters given by $L_5 = 18.07\text{mm}$, $W_3 = 0.20\text{mm}$, $L_9 = 11.57\text{mm}$, $W_5 = 0.93\text{mm}$, $L_{10} = 18.115\text{mm}$, $W_6 = 0.90\text{mm}$, $L_{13} = 18.07\text{mm}$, $W_7 = 1.50\text{mm}$. In addition, each strip line was separated with different parameters given by $L_4 = 2.10\text{mm}$, $L_6 = 3.18\text{mm}$, $L_8 = 1.06\text{mm}$, $L_{10} = 1.46\text{mm}$, $L_{12} = 2.40\text{mm}$.

3.4 Results and Discussions

In this project all the measurements are done by using Rohde & Schwarz Vector Network Analyzer ZVB8. The result of dual-mode dual-band microstrip bandpass filter is shown in Figure 3.1.

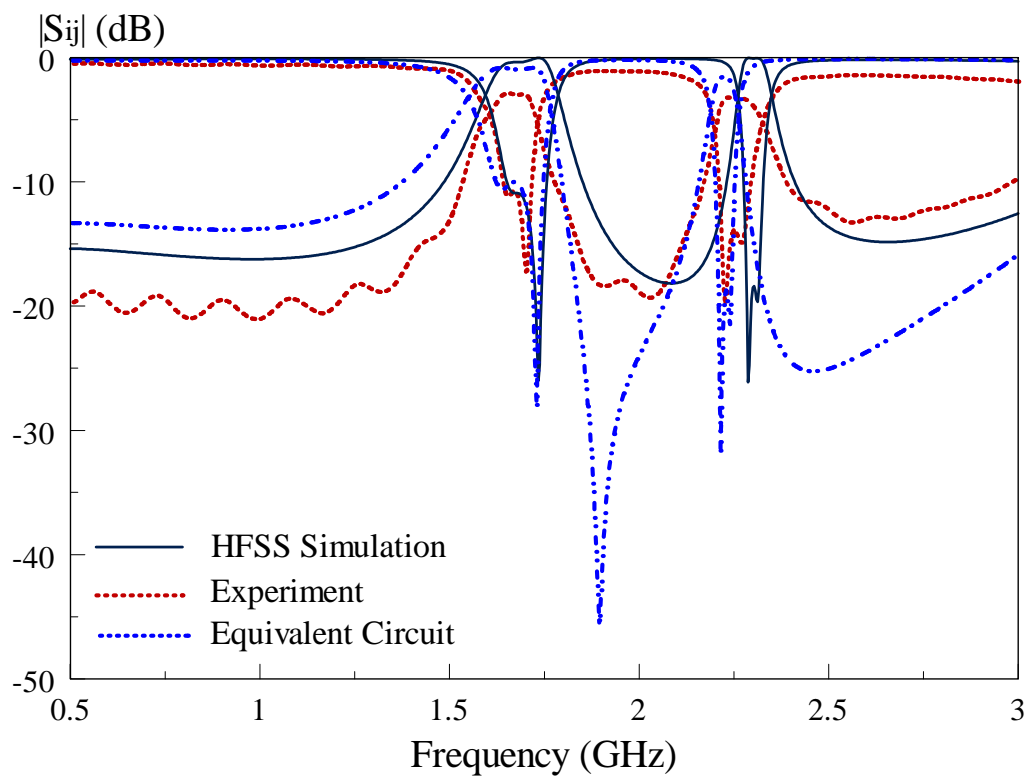


Figure 3.3: Measured and simulated S_{11} and S_{21} of dual-mode dual-band microstrip bandpass filter

Figure 3.3 shows the simulated and measured return losses and insertion losses. From the figure, the measured center frequency is 1.655 GHz, which is very close to the simulated value of 1.69 GHz (error 2.07%). The measured and simulated 3-dB bandwidths ($|S_{11}| \leq -10$ dB) are given by 9.09% and 12.79%, respectively. Also shown in the figure are the simulated S_{11} and S_{21} by using the network model. With

reference to the figure, the measured center frequency is 1.65 GHz, which is very close to the simulated value of 1.69 GHz (error 2.37%). The measured 3-dB bandwidth ($|S_{11}| \leq -10$ dB) by using network model is given by 10.40%. With reference to the figure, the models predict the S_{11} and S_{21} reasonably well.

The error might caused by the gap distance. From the simulation design the capacitive coupling gap is 0.01 mm. However, such narrow gap is difficult to fabricate by the equipment in the laboratory. Few Duroid 6006 substrates have been fabricated and experiment. At the end of the day this is the best result the author able to collect.

CHAPTER 4

PARAMETER ANALYSIS

4.1 Case Studies

In the case studies, only one of the filter parameters will be changed at one time and the result will be studied for better improvement. For instance, gap between the resonators changed to 0.1 mm while other parameters remain the same. In this chapter, gap results have been studied. For comparison purpose the frequency range has been set to 0.5 to 3 GHz.

4.2 Gap

At first the affect of the gap to the filter response has been studied. The author has study based on the proposed design in Figure 3.1. The parameter analysis for the gap distances is shown in the Figure 4.1 - 4.17.

4.3 Width

Besides, the width of the filter response has also been studied. The author has study based on the proposed design in Figure 3.1. The parameter analysis for the width of the strip lines is shown in the Figure 4.18 - 4.34.

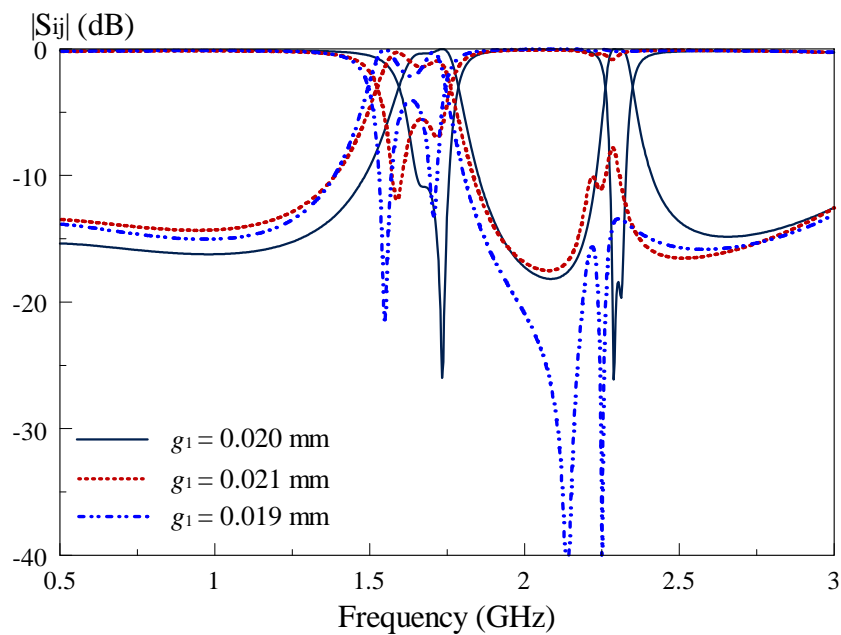


Figure 4.1: Response of Case Studies I

From the Figure 4.1, it can be noticed that the second passband has been deteriorate; neither the gap distance of g_1 is increase or decrease.

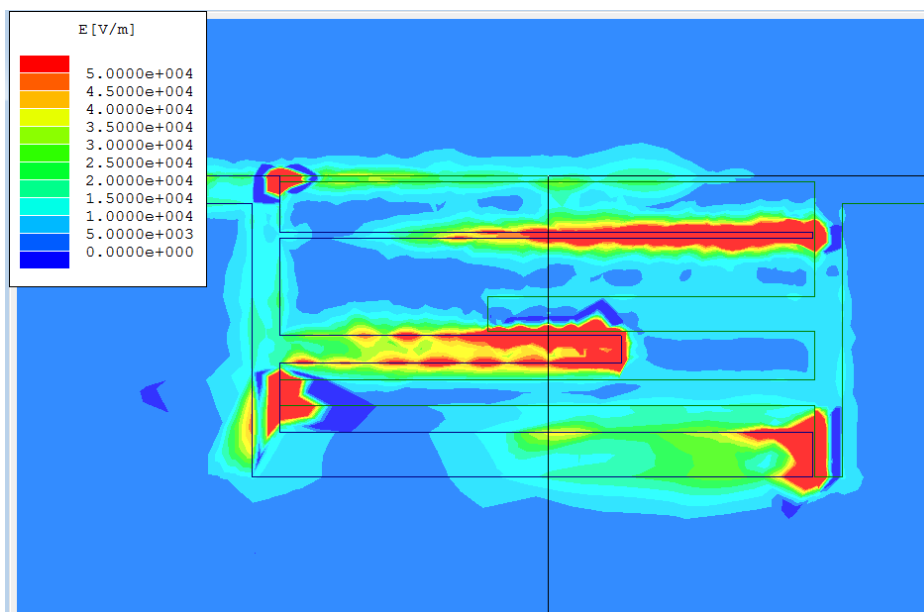


Figure 4.2: The electric field when $g_1=0.021\text{mm}$

By observing the Figure 4.2, the second passband obviously is influenced by the g_1 . Besides g_1 , the second passband also influence by gap distances of g_2 , g_5 and

also g_6 . At the same time, the gap distance between the third and fourth strip line influenced the second passband as well.

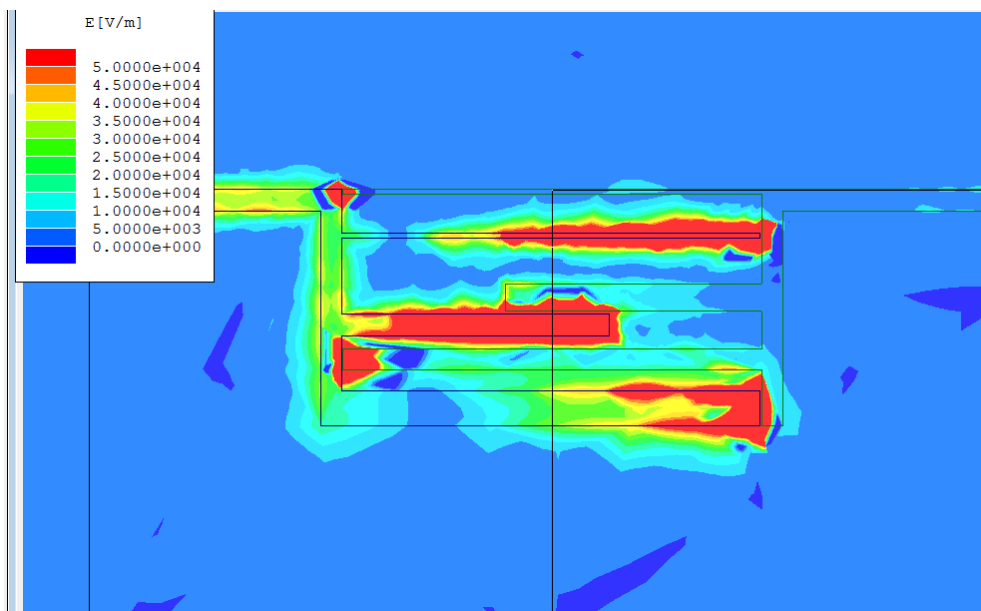


Figure 4.3: The electric field when $g_1=0.19\text{mm}$

By observing the Figure 4.3, the second passband obviously is influenced by the g_1 . Besides g_1 , the second passband also influence by changing the gap distances of g_2 , g_5 and also g_6 . At the same time, the gap distance between the third and fourth strip line influenced the second passband as well.

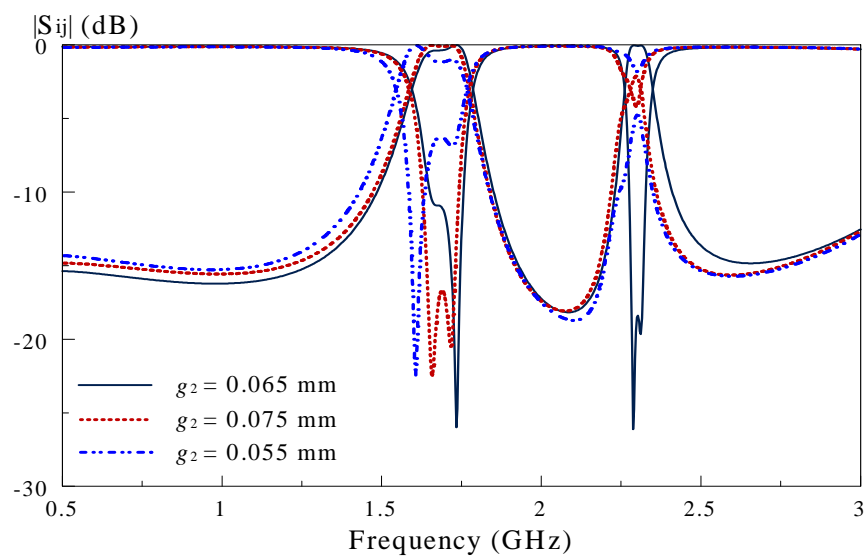


Figure 4.4: Response of Case Study II

From the Figure 4.4, the second passband has been influenced by the gap distance of g_2 . The first passband do not influence much by the changes of the gap distance, g_2 . Hence , both passband are optimized at 0.065mm.

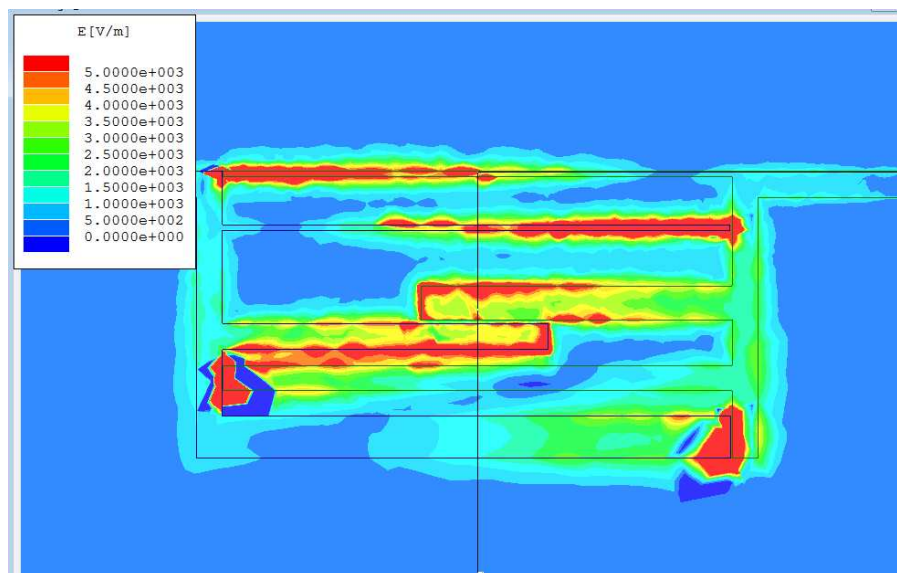


Figure 4.5: The electric field when $g_2= 0.075\text{mm}$

By observing the Figure 4.5, the second passband obviously is influenced by the g_2 . Besides g_2 , the second passband also influence by changing the gap distances of g_1 , g_5 and also g_6 . At the same time, the gap distance between the third and fourth strip lines influenced the second passband as well.

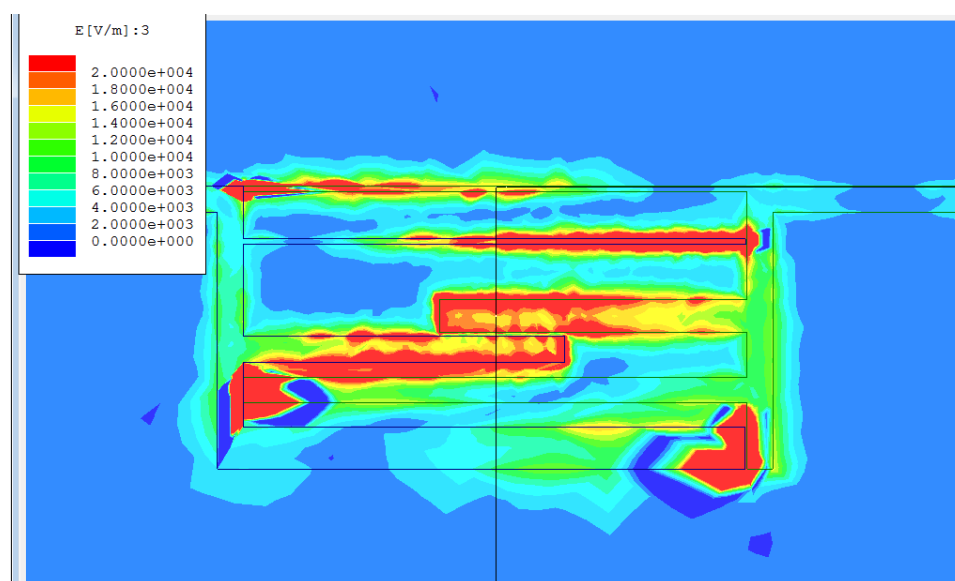


Figure 4.6: The electric field when $g_2= 0.055\text{mm}$

By observing the Figure 4.6, the second passband obviously is influenced by the g_2 . Besides g_2 , the second passband also influence by changing the gap distances of g_1 , g_5 and also g_6 . At the same time, the gap distance between the third and fourth strip lines influenced the second passband as well.

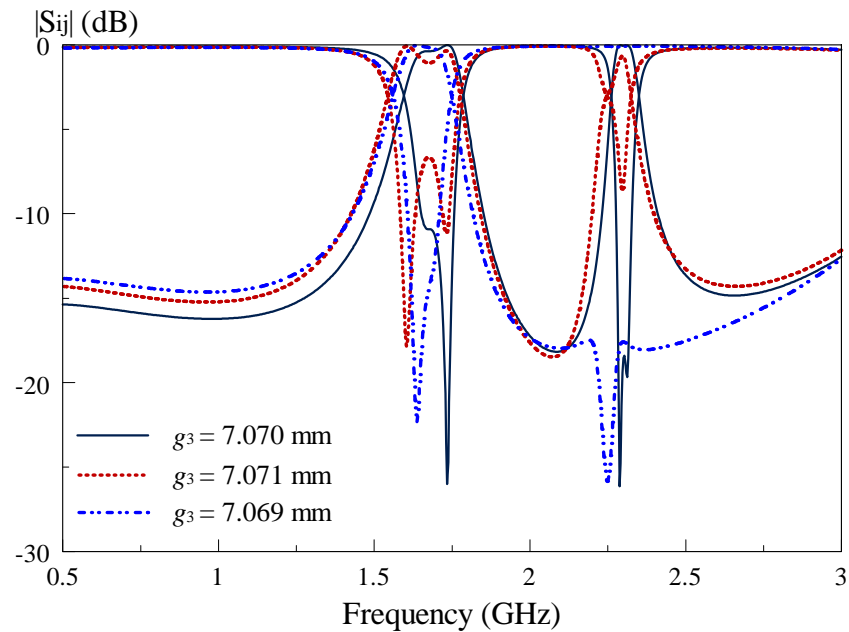


Figure 4.7: Response of Case study III

From the Figure 4.7, the second passband deteriorated faster at $g_3 = 7.071$ mm. When the gap distance was adjusted equal to 7.069 mm, the second passband do not deteriorated much. Hence, both passbands are optimized at 0.065 mm.

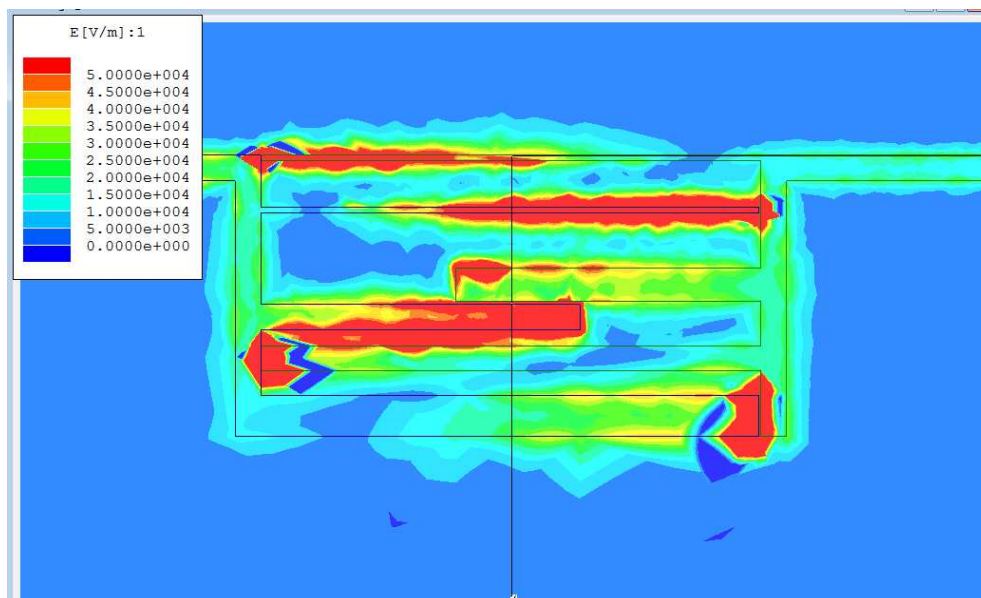


Figure 4.8: The electric field when $g_3=7.071\text{mm}$

By observing the Figure 4.8, the second passband obviously is influenced by the g_3 . Besides g_3 , the second passband also influence by changing the gap distances of g_1 , g_2 , g_5 and also g_6 . At the same time, the gap distance between the third and fourth strip lines influenced the second passband as well.

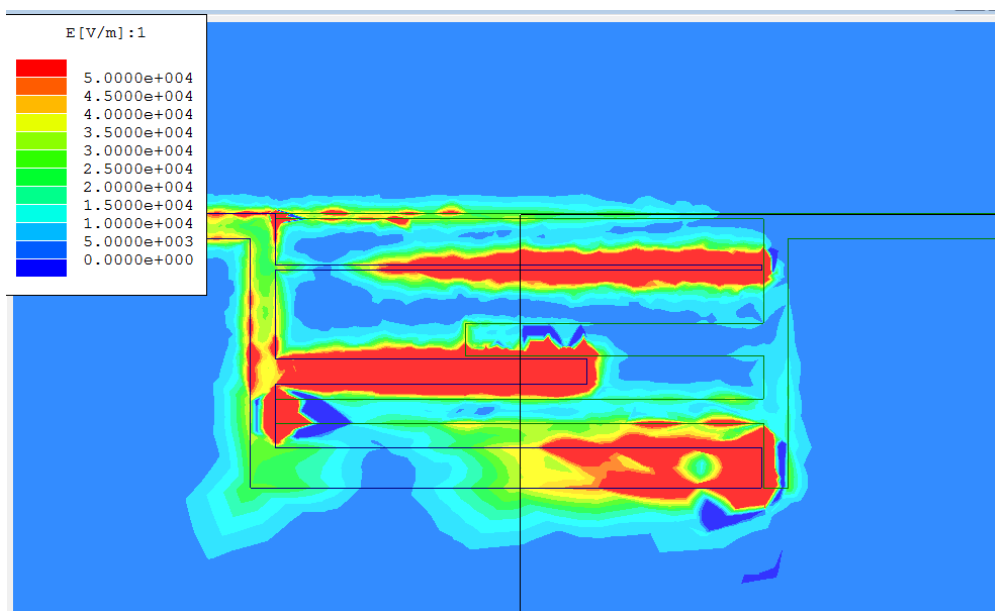


Figure 4.9: The electric field when $g_3 = 7.069\text{mm}$

By observing the Figure 4.9, the second passband obviously is influenced by the g_3 . Besides g_3 , the second passband also influence by changing the gap distances

of g_1 , g_2 , g_5 and also g_6 . At the same time, the width of the second and fourth strip lines influenced the second passband as well.

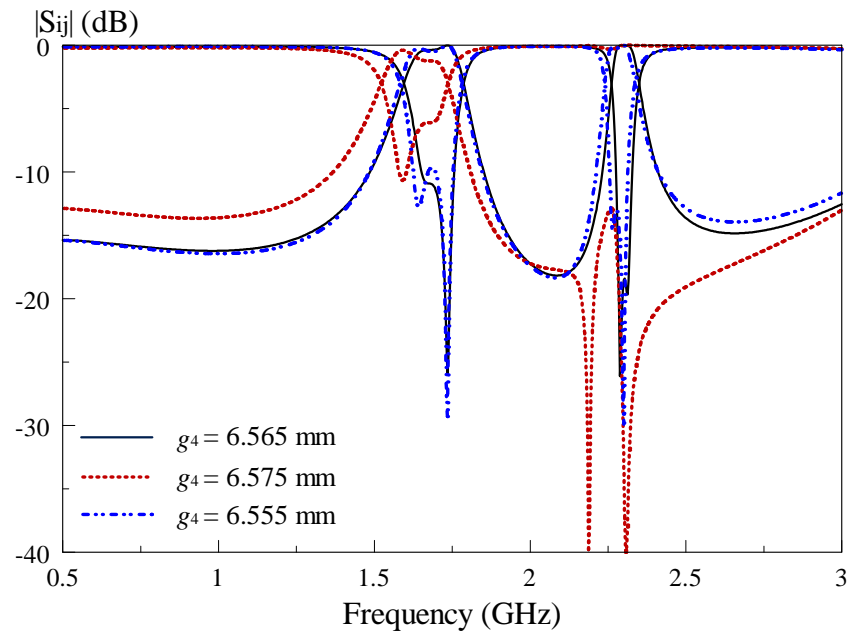


Figure 4.10: Response of Case Study IV

From the Figure 4.10, the first and second passband deteriorated faster at $g_4=6.575\text{mm}$. However, the first and the second passband do not influence much when the gap distance $g_4=6.555\text{mm}$. Hence, both passbands are optimized at 6.565mm .

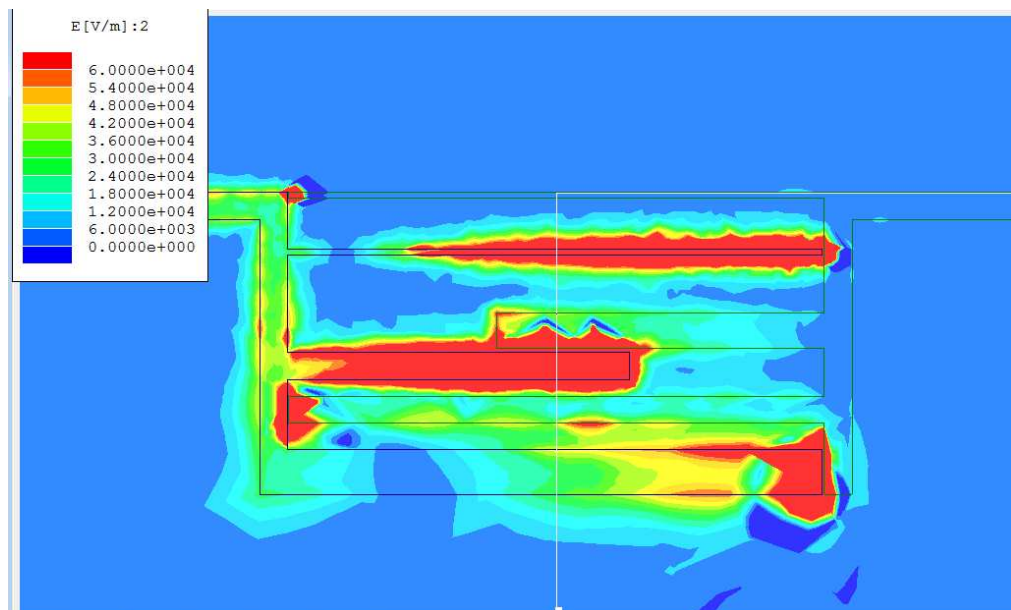


Figure 4.11: The electric field when $g_4=6.575\text{mm}$

By observing the Figure 4.11, the second passband obviously is influenced by the g_4 . Besides g_4 , the second passband also influence by changing the gap distances of g_1 , g_2 , g_5 and also g_6 . At the same time, the width of the second and third strip lines influenced the second passband as well.

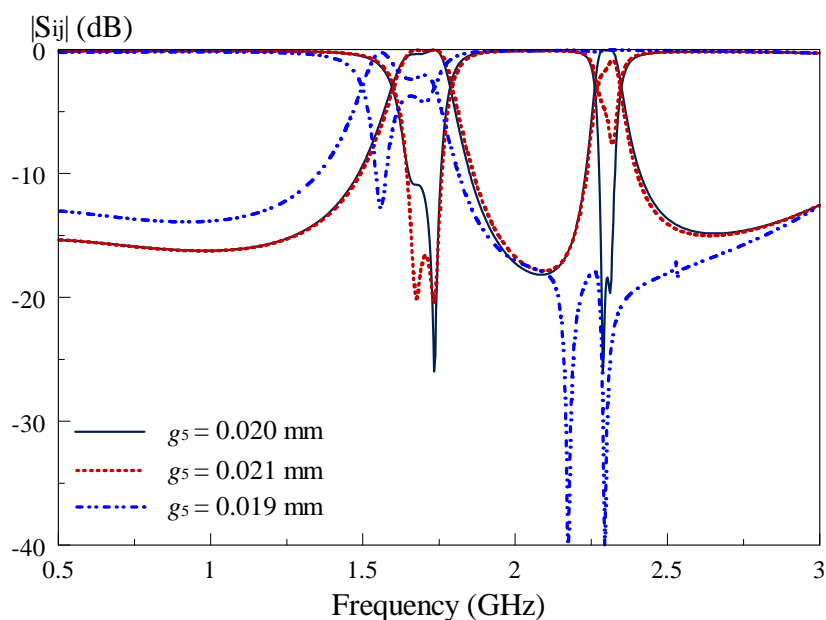


Figure 4.12: Response of Case Study V

From the Figure 4.12, the second passband degrades faster at $g_5= 0.019\text{mm}$. However, the first and the second passband do not influence much when the gap distance $g_5= 0.021\text{mm}$. Hence, both passbands are optimized at 0.020mm .

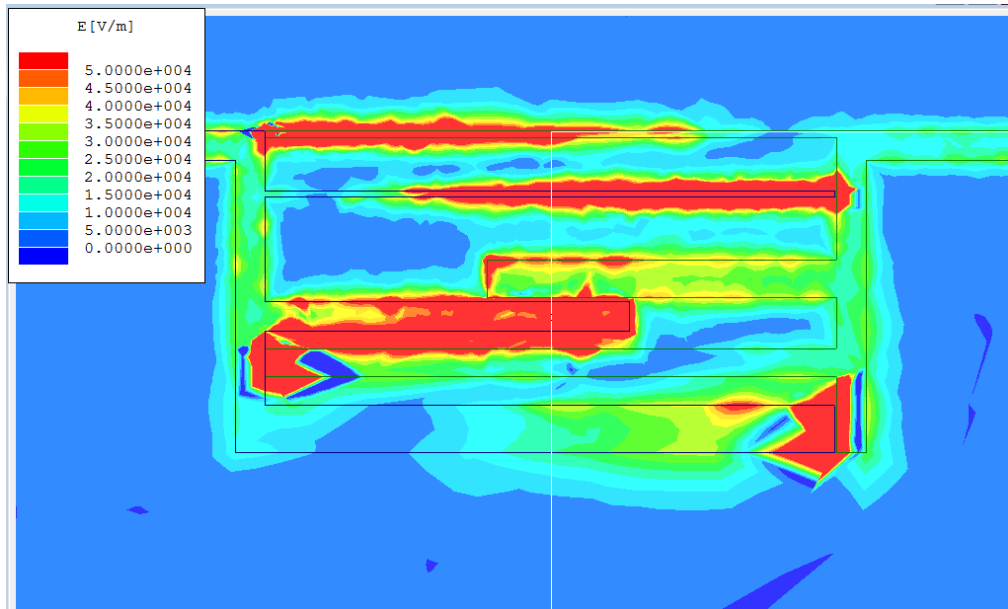


Figure 4.13: The electric field when $g_5=0.021\text{mm}$

By observing the Figure 4.13, the second passband obviously is influenced by the g_5 . Besides g_5 , the second passband also influence by changing the gap distances of g_1 , g_2 , g_5 and also g_6 . At the same time, the width of the first, second and fourth strip lines influenced the second passband as well.

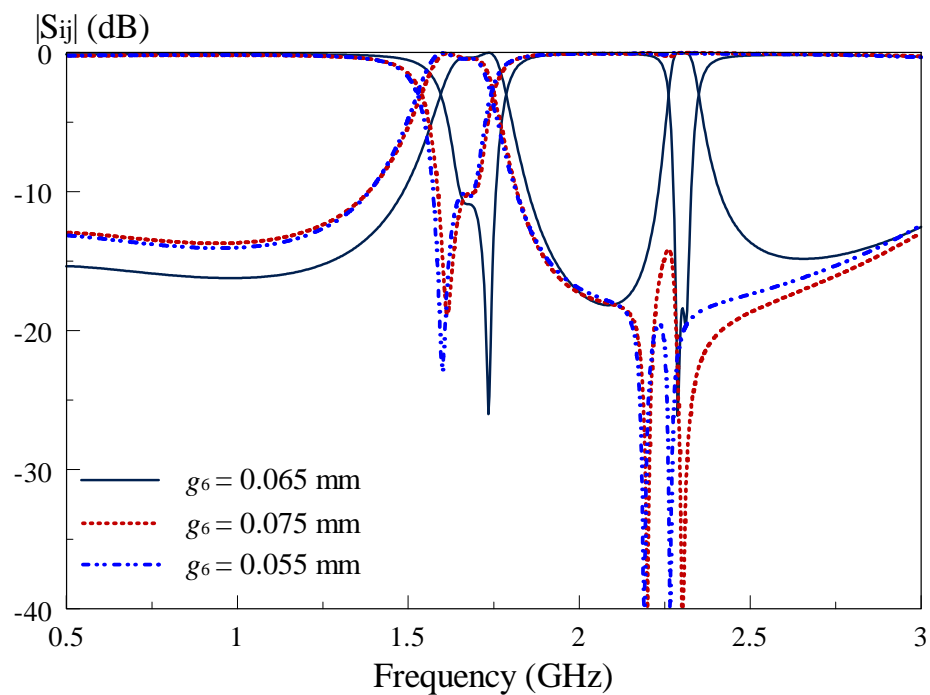


Figure 4.14: Response of Case Study VI

From the Figure 4.14, the second passband degrades faster when the gap distance of $g_6=0.075\text{mm}$ and $g_6=0.055\text{mm}$. Hence, both passband are optimized at 0.065mm .

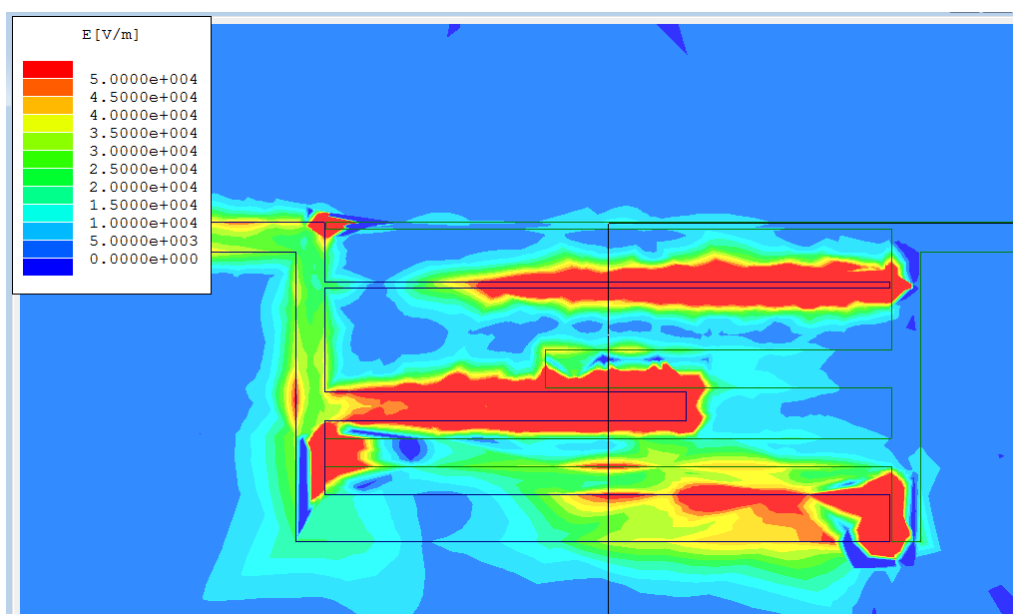


Figure 4.15: The electric field when $g_6=0.075\text{mm}$

By observing the Figure 4.15, the second passband obviously is influenced by the g_6 . Besides g_6 , the second passband also influence by changing the gap distances of g_1 , g_2 , g_5 and also g_6 . At the same time, the width of the second, fourth and sixth strip lines influenced the second passband as well.

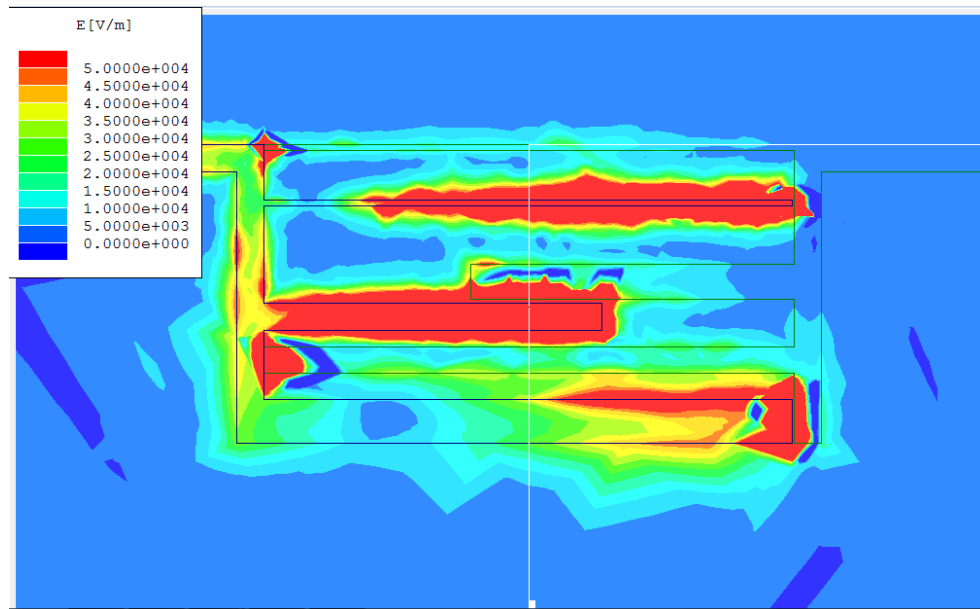


Figure 4.16: The electric field when $g_6=0.055\text{mm}$

By observing the Figure 4.15, the second passband obviously is influenced by the g_6 . Besides g_6 , the second passband also influence by changing the gap distances of g_1 , g_2 , g_5 and also g_6 . At the same time, the width of the second, fourth and sixth strip lines influenced the second passband as well.

Generally, smaller gap able to create a stronger capacitive coupling between the resonators. From the all the figures above show the upper passband and lower passband are influenced by the changes of the gaps. However, at the same time, the width of the strip lines also influenced the motion of electromagnetic flow between the strip lines.

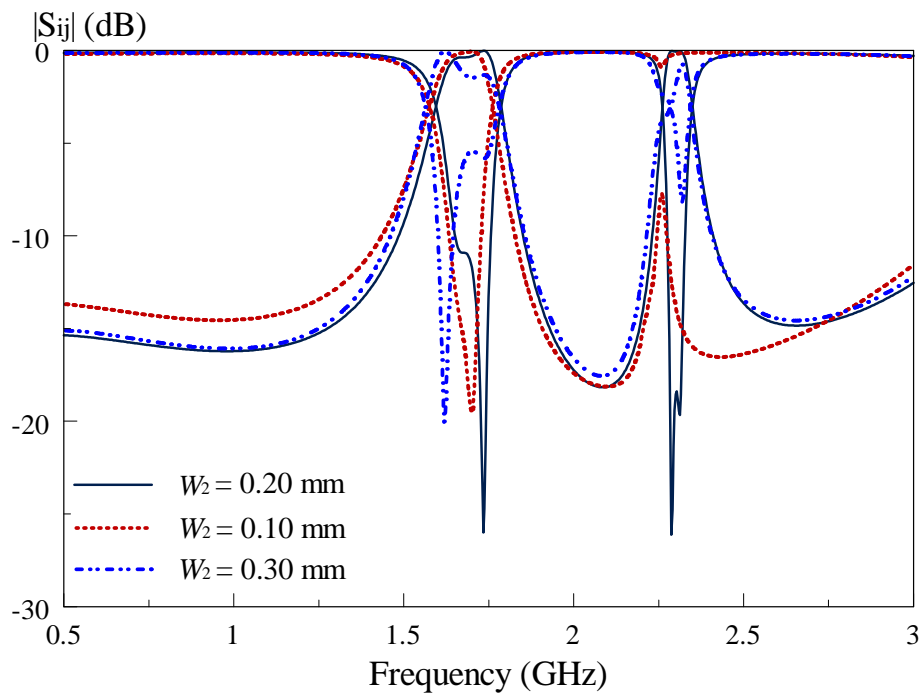


Figure 4.17: Response of Case Study VII

From the Figure 4.17, it can be observed that the second passband degrades faster when the width of the first strip line $W_2=0.10\text{mm}$ compared to its counterpart. Hence, both passband are optimized at 0.20mm .

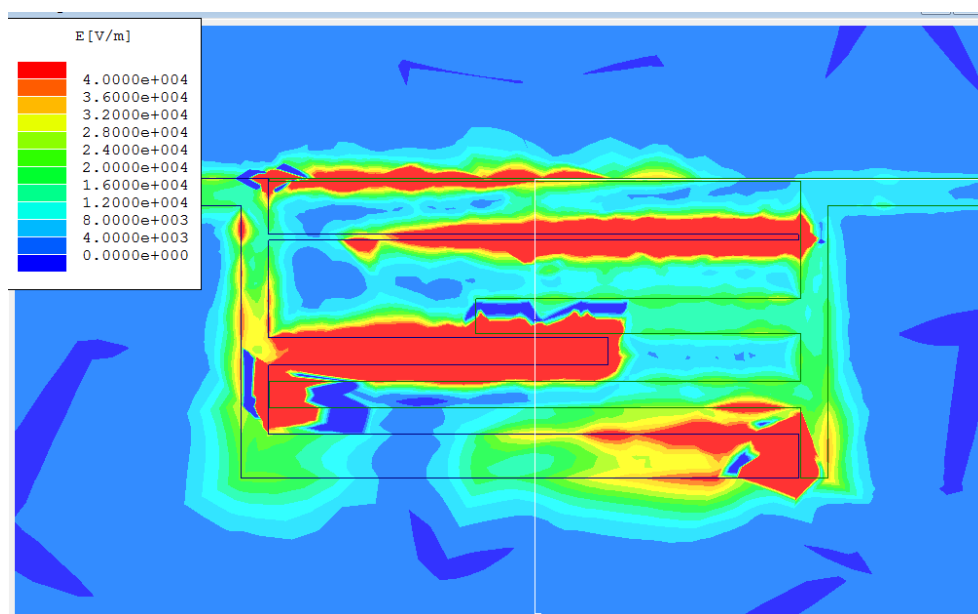


Figure 4.18: The electric field when $W_2=0.10\text{mm}$

By observing the Figure 4.18, the second passband vanishes obviously as it is influenced by the W_2 . Besides W_2 , the second passband also influence by changing the width of the W_3 , W_5 , and W_6 . At the same time, the gap distances of the g_1 , g_2 , g_4 , g_5 and also g_6 influenced the second passband as well.

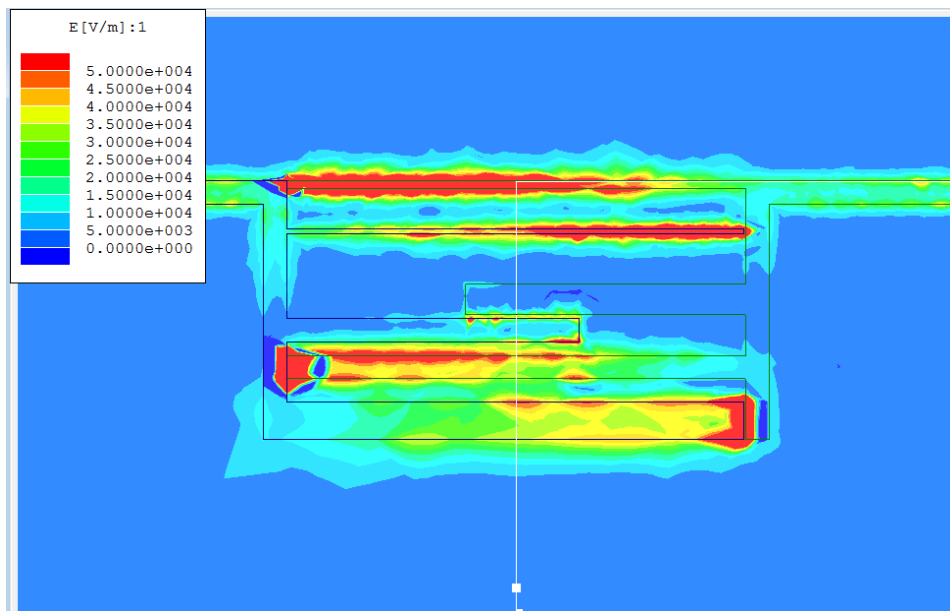


Figure 4.19: The electric field when $W_2=0.30\text{mm}$

By observing the Figure 4.19, the first and second passbands vanish obviously as it is influenced by the W_2 . Besides W_2 , the first passband also influence by changing the width of the W_3 , W_5 , and W_6 . At the same time, the gap distances of the g_1 , g_2 , g_4 , g_5 and also g_6 influenced the first and second passbands as well.

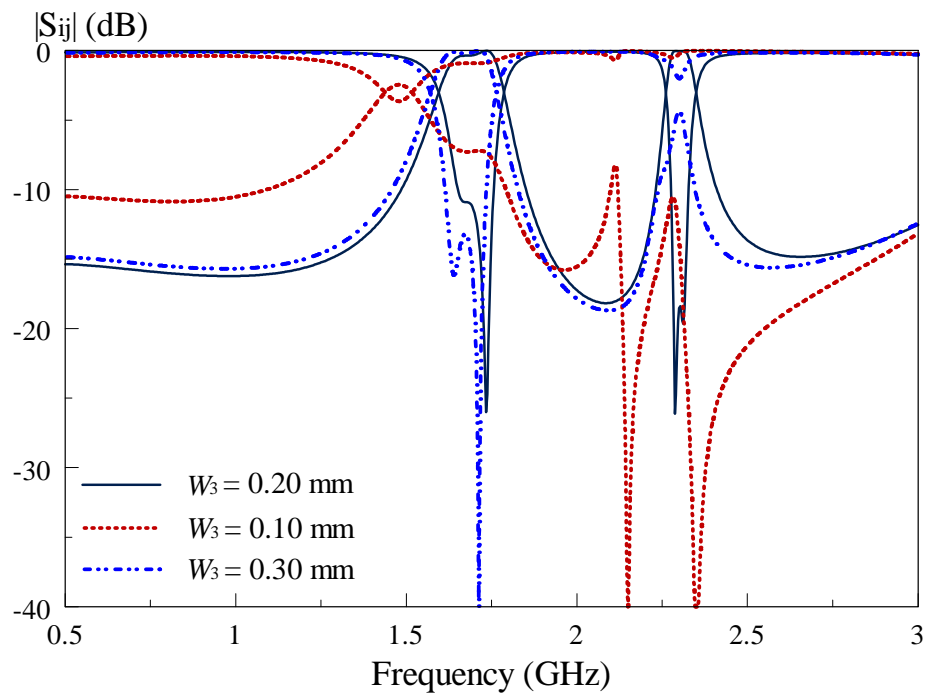


Figure 4.20: Response of Case Study VIII

From the Figure 4.20, it can be observed that the first and second passbands degrade faster when the width of the second strip line $W_3=0.10\text{mm}$ compared to its counterpart. The second passband is influenced by the changes of the width, $W_3=0.30\text{mm}$. Hence, both passband are optimized at 0.20mm .

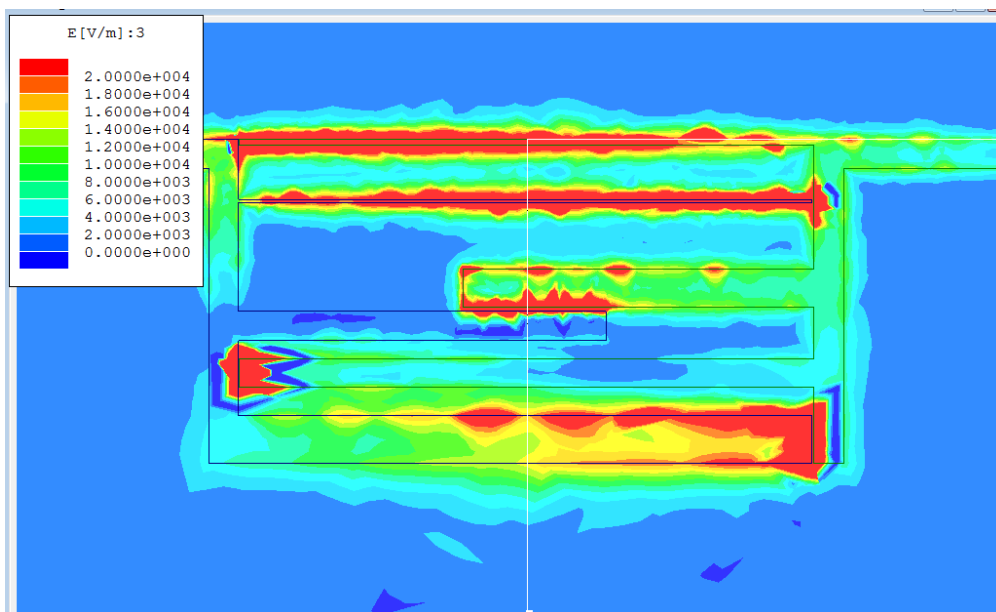


Figure 4.21: The electric field when $W_3=0.10\text{mm}$

By observing the Figure 4.21, both passbands vanish obviously as it is influenced by the W_3 . Besides W_3 , both passbands are also influence by changing the width of the W_2 , W_4 , W_5 , W_6 and W_7 . At the same time, the gap distances of the g_1 , g_2 , g_5 and g_6 influenced the first and second passbands as well.

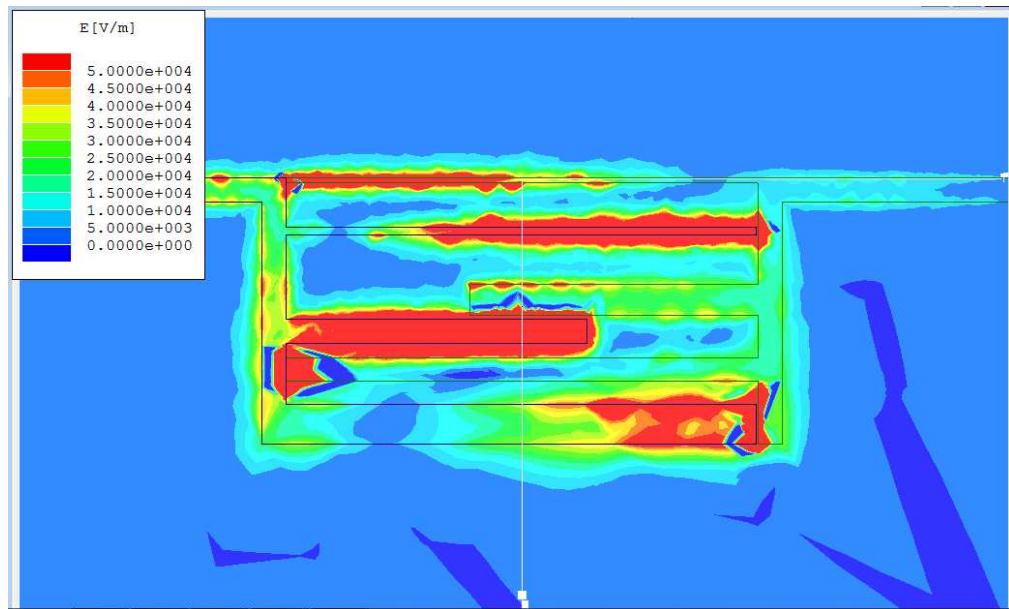


Figure 4.22: The electric field when $W_3=0.30\text{mm}$

By observing the Figure 4.22, both passbands vanish obviously as it is influenced by the W_3 . Besides W_3 , both passbands are also influence by changing the width of the W_2 , W_4 , W_5 , W_6 , and W_7 . At the same time, the gap distances of the g_1 , g_2 , g_5 and g_6 influenced the first and second passbands as well.

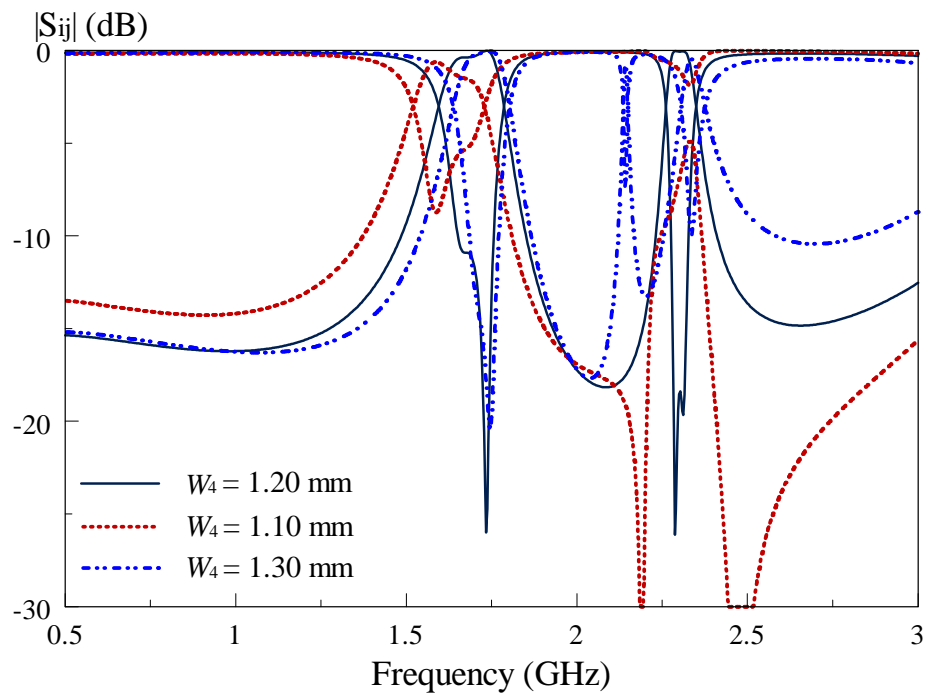


Figure 4.23: Response of Case Study VIII

From the Figure 4.23, it can be observed that the second passband degrade faster when the width of the third strip line $W_4=1.10\text{mm}$. Also, the first and the second passbands are vanished when the $W_4=1.30\text{mm}$. Hence, both passband are optimized at 1.20mm .

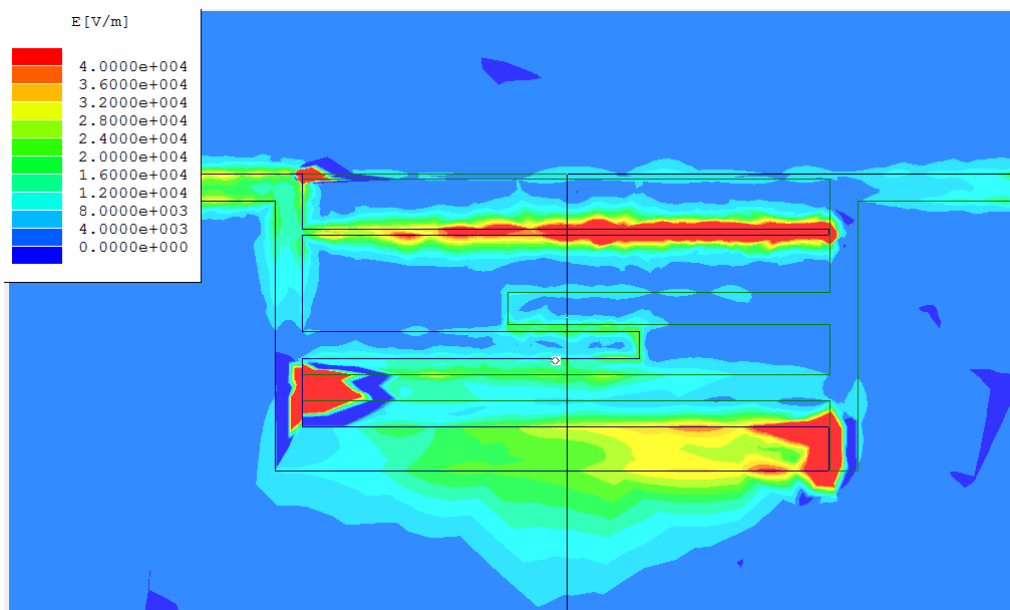


Figure 4.24: The electric field when $W_4=1.10\text{mm}$

By observing the Figure 4.24, the second passband vanishes obviously as it is influenced by the W_4 . Besides W_4 , both passbands are also influence by changing the width of the W_2 , W_3 , W_6 , and W_7 . At the same time, the gap distances of the g_1 , g_2 , g_5 and g_6 influenced the first and second passbands as well.

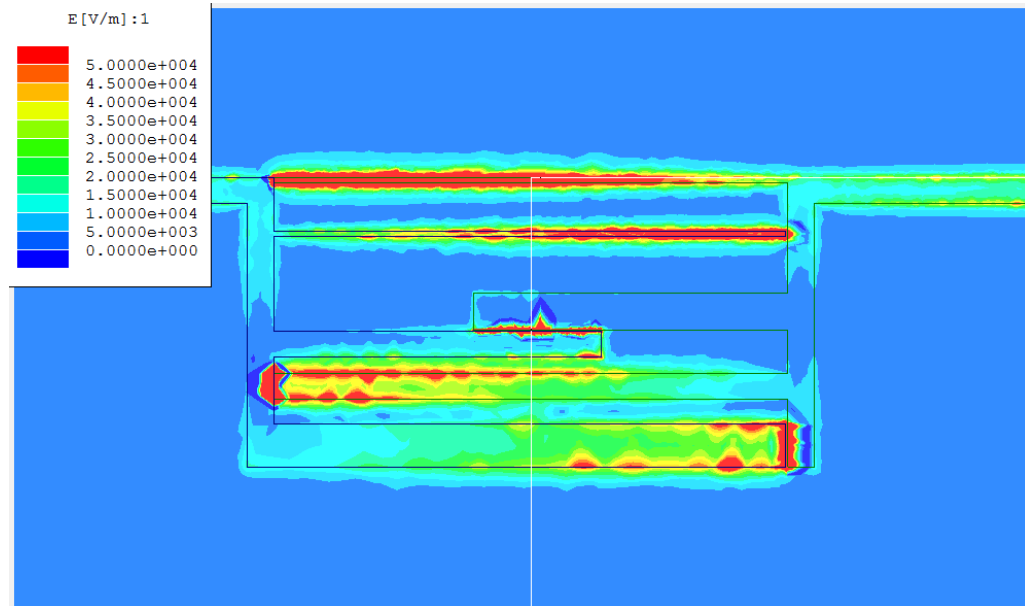


Figure 4.25: The electric field when $W_4=1.30\text{mm}$

By observing the Figure 4.25, the second passband vanishes obviously as it is influenced by the W_4 . Besides W_4 , both passbands are also influence by changing the width of the W_2 , W_3 , W_5 , W_6 , and W_7 . At the same time, the gap distances of the g_1 , g_2 , g_5 and g_6 influenced the first and second passbands as well.

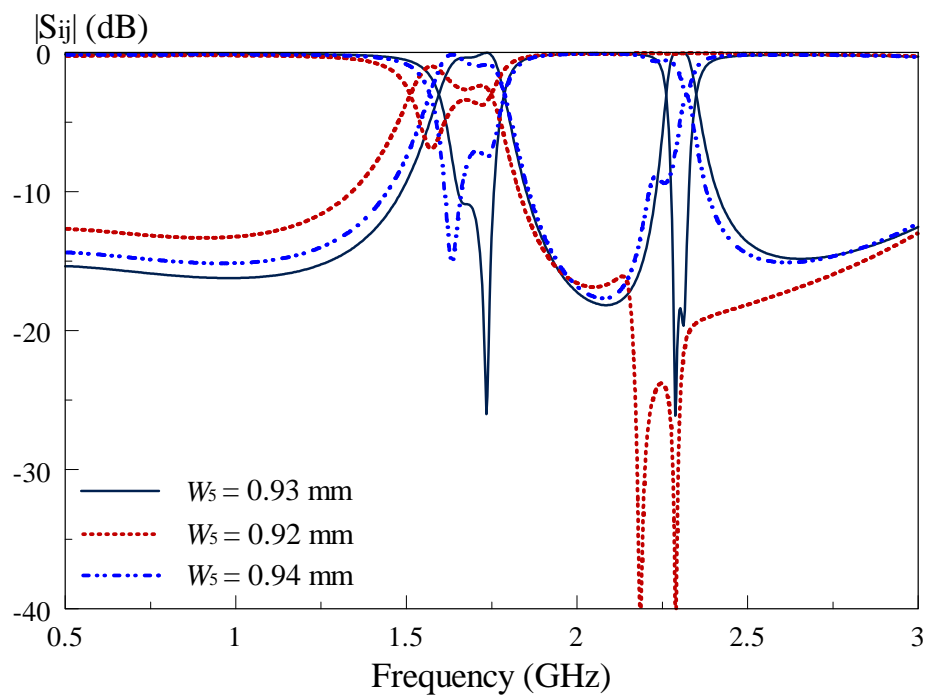


Figure 4.26: Response of Case Study X

From the Figure 4.26, it can be observed that the second passband degrade faster when the width of the fourth strip line $W_5=0.92\text{mm}$. Also, the first and the second passbands are vanished when the $W_4=0.94\text{mm}$. Hence, both passband are optimized at 0.93mm .

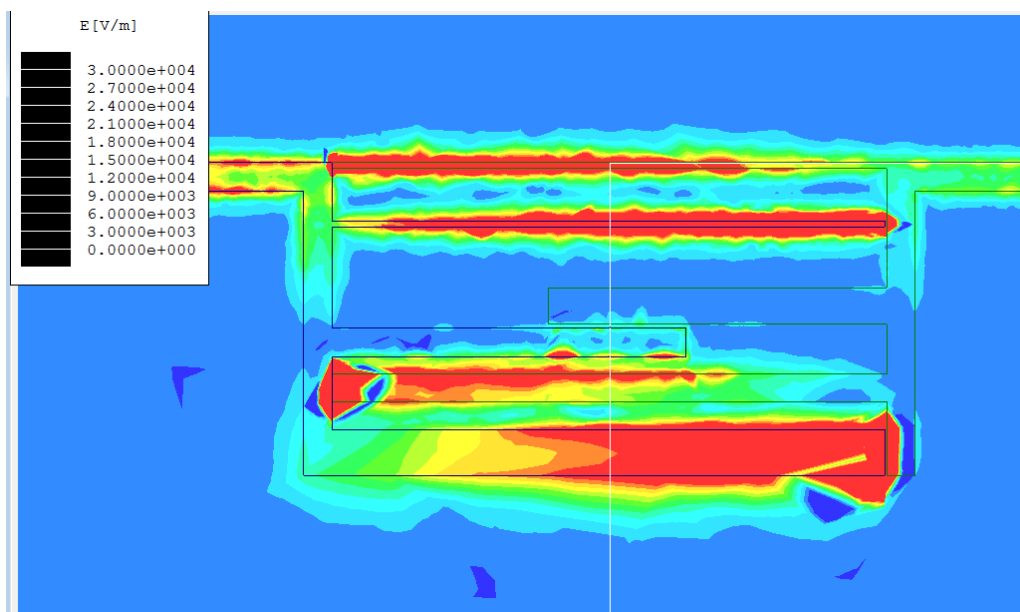


Figure 4.27: The electric field when $W_5=0.92\text{mm}$

By observing the Figure 4.27, the second passband vanishes obviously as it is influenced by the W_5 . Besides W_5 , both passbands are also influence by changing the width of the W_2 , W_3 , W_6 , and W_7 . At the same time, the gap distances of the g_1 , g_2 , g_5 and g_6 influenced the first and second passbands as well.

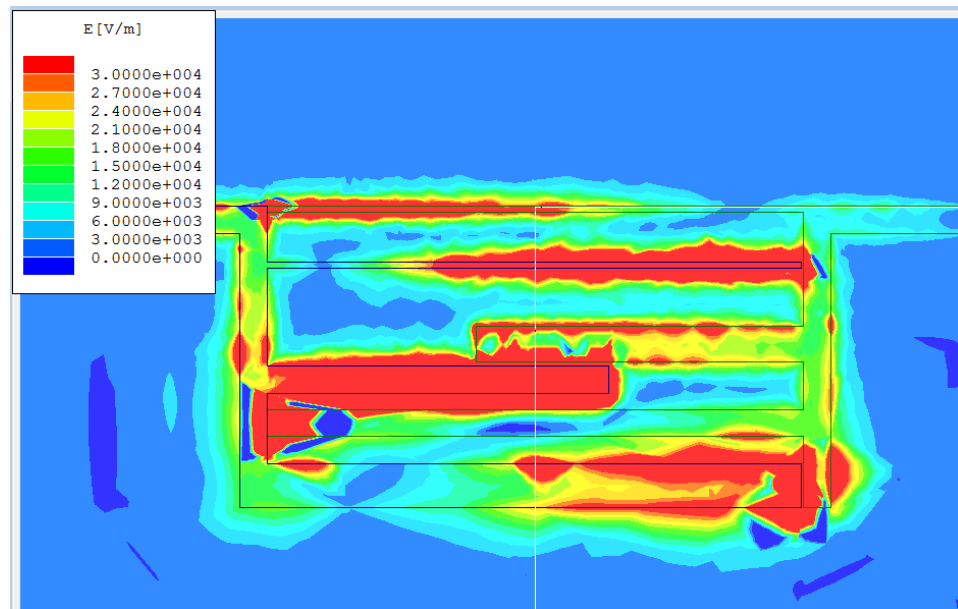


Figure 4.28: The electric field when $W_5=0.94\text{mm}$

By observing the Figure 4.28, the second passband vanishes obviously as it is influenced by the W_5 . Besides W_5 , both passbands are also influence by changing the width of the W_2 , W_3 , W_4 , W_6 , and W_7 . At the same time, the gap distances of the g_1 , g_2 , g_3 , g_4 , g_5 and g_6 influenced the first and second passbands as well.

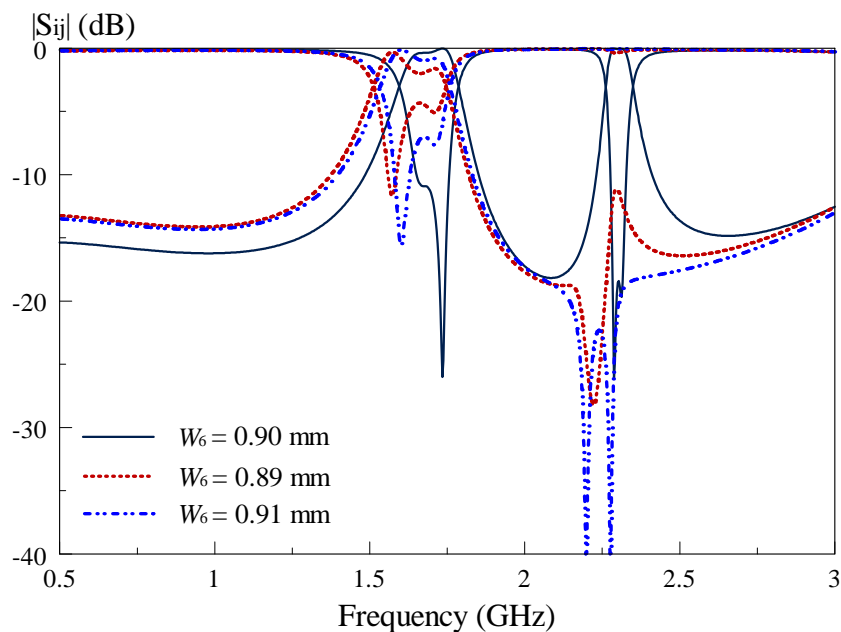


Figure 4.29: Response of Case study XI

From the Figure 4.29, it can be observed that the first and second passbands degrade faster when the width of the fifth strip line is either $W_6=0.89\text{mm}$ or $W_6=0.91\text{mm}$. Hence, both passband are optimized at 0.90mm .

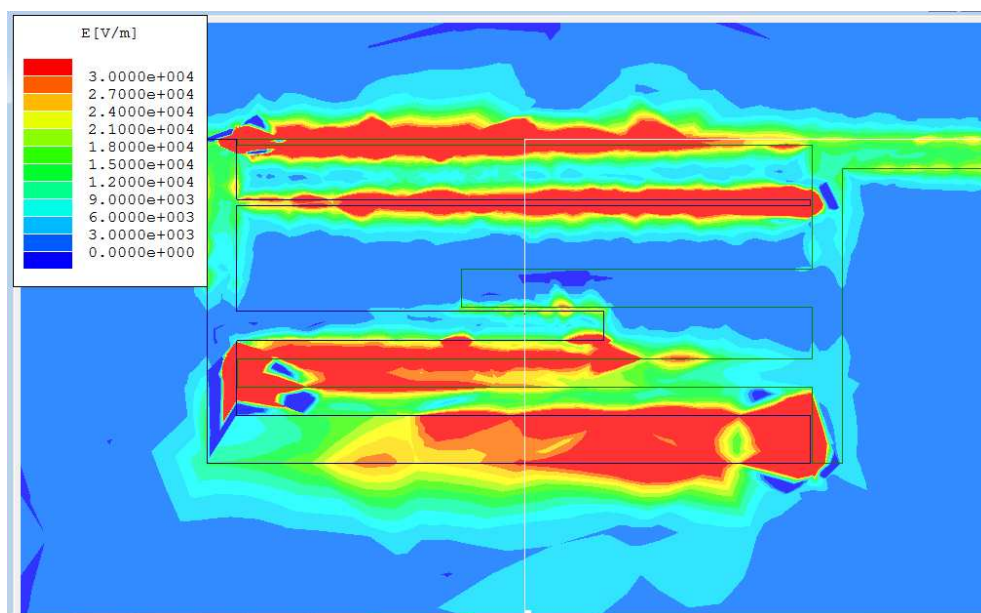


Figure 4.30: The electric field when $W_6=0.89\text{mm}$

By observing the Figure 4.30, the second passband vanishes obviously as it is influenced by the W_6 . Besides W_6 , both passbands are also influence by changing the

width of the W_2 , W_3 , W_6 , and W_7 . At the same time, the gap distances of the g_1 , g_2 , g_5 and g_6 influenced the first and second passbands as well.

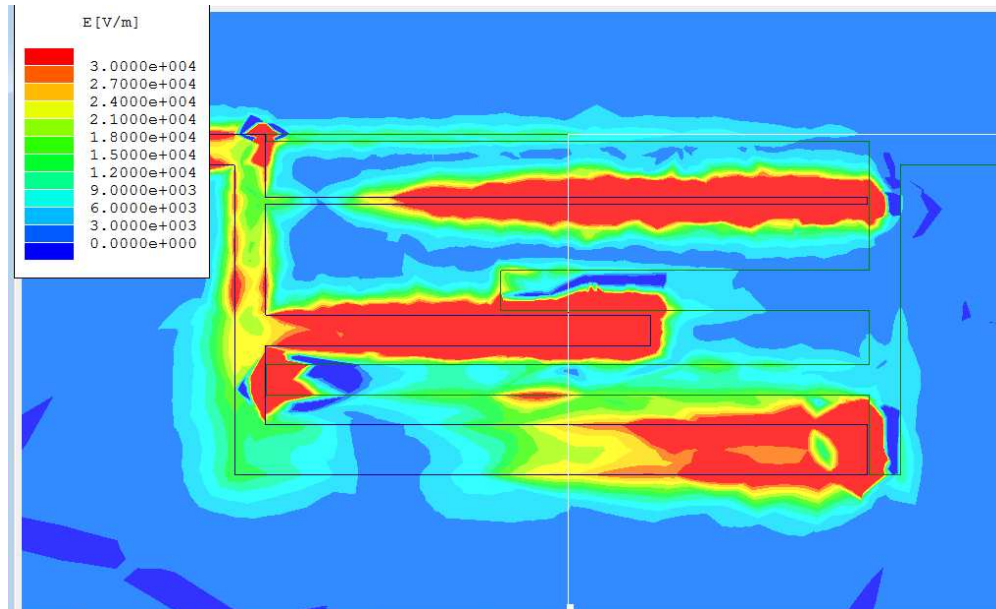


Figure 4.31: The electric field when $W_6=0.91\text{mm}$

By observing the Figure 4.31, the second passband vanishes obviously as it is influenced by the W_6 . Besides W_6 , both passbands are also influence by changing the width of the W_2 , W_3 , W_5 , W_6 , and W_7 . At the same time, the gap distances of the g_1 , g_2 , g_4 , g_5 and g_6 influenced the first and second passbands as well.

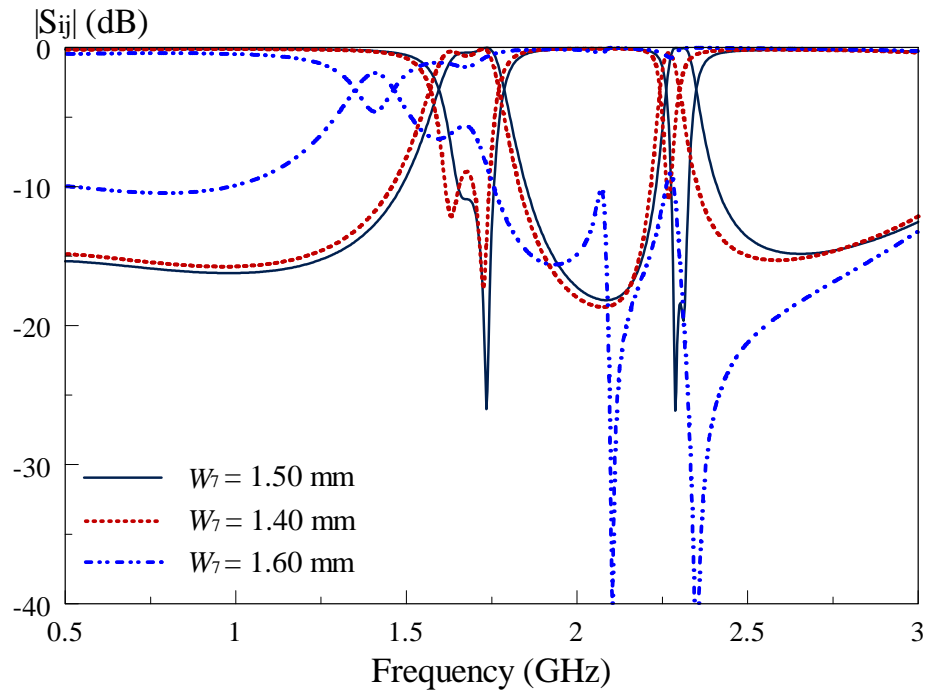


Figure 4.32: Response of Case Study XII

From the Figure 4.32, it can be observed that the second passband vanishes when the width of the sixth strip line is either $W_7=1.40$ mm or $W_6=1.60$ mm. Hence, both passband are optimized at 1.50mm.

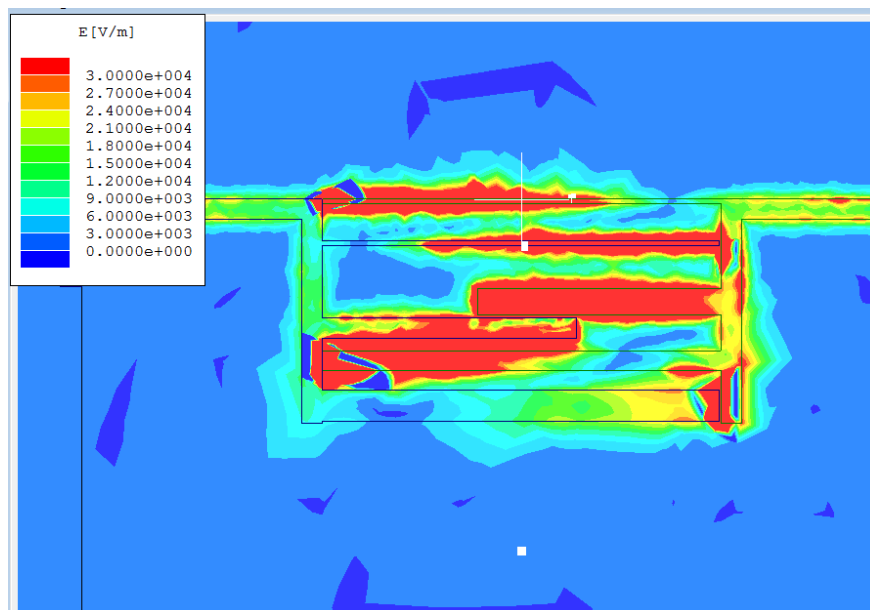


Figure 4.33: The electric field when $W_7=1.40$ mm

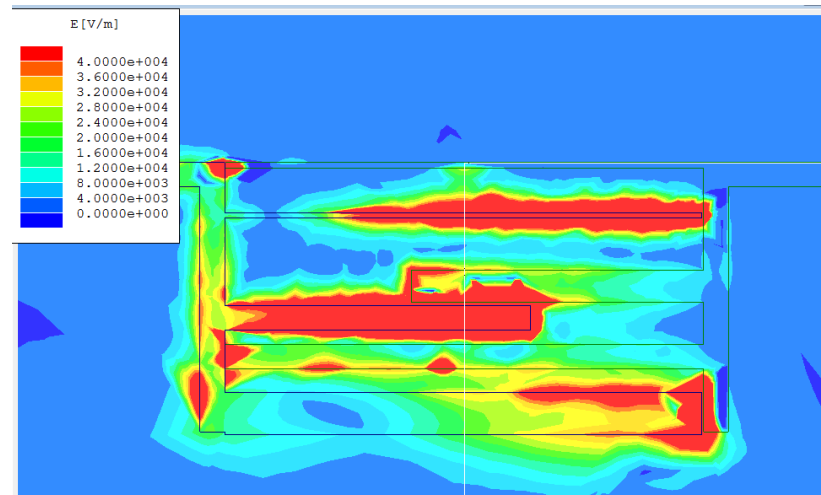


Figure 4.34: The electric field when $W_7=1.60\text{mm}$

By observing the Figure 4.33 and 4.34, the second passband vanishes obviously as it is influenced by the W_7 . Besides W_7 , both passbands are also influence by changing the width of the W_2 , W_3 , W_4 , W_5 , and W_6 . At the same time, the gap distances of the g_1 , g_2 , g_3 , g_4 , g_5 and g_6 influenced the first and second passbands as well.

CHAPTER 5

CONCLUSION AND RECOMMENDATIONS

5.1 Conclusion

As a conclusion, microstrip band pass filters have been studied. An inter-digit microstrip dual-mode dual-band band pass filter has been designed and demonstrated in this project. The simulated results based on HFSS version 8 shown reasonably well with measurements. With the experience had in this project, writer able to design filters or antennas based on HFSS simulation software and measured the results with VNA in laboratory. Thus, the objective of this project has been achieved.

5.2 Recommendation

Since the gaps will affect the filter response, every 0.01mm changes will bring different response to the filter. Thus, it has never been any easy to fabricate the microstrip fingers with limited facilities in the laboratory. It is advisable, to fabricate the small gaps between resonators, it is better to have a laser machining in the laboratory. This will achieve high machining accuracy with tight tolerance and ease the work of fabrication process.

Besides, the filter is made up of a number of interleaved microstrip fingers coupled together as shown in Fig. 3.1. The maximum value of an inter-digital capacitor is limited by its physical size, and its maximum usable operating frequency

is limited by the distributed nature of the fingers. Therefore, the performance of the filter can be further improved by increasing the number of fingers. They are ideal as tuning, coupling and matching elements, where small capacitor values are required and precise values are necessary.

REFERENCES

- Band Pass Filter. (n.d.) Wikipedia. Retrieved August 27, 2009 from http://en.wikipedia.org/wiki/Band_pass_filter
- Mohamed Azaga1, Masuri Othman, “ Design of Parallel-Coupled Microstrip Line Band Pass Filter (BPF) for Ultra-Wide Band (UWB) Applications” IEEE International Conference on Computer and Communication Engineering., pp. 280-283, 2008
- Lei Zhu, Boon Chai Tan, and Siang Juay Quek, “Miniaturized Dual-Mode Band pass filter Using Inductively Loaded Cross-Slotted Patch Resonator” IEEE Microwave and Wireless Components Letters., vol. 15, pp. 22-24, 2005
- Yatendra Kumar Singh and Ajay Chakrabartyand, “Miniaturized Dual-Mode Circular Patch Bandpass Filters With Wide Harmonic Separation” IEEE Microwave and Wireless Components Letters., vol. 18, pp. 584-586, 2008
- Jia-Sheng Hong and Michael J. Lancaster, “ Microstrip Triangular Patch Resonator Filters” IEEE MTT-S Digest, pp. 331-334, 2000
- H.-K. Chiou, and C.-Fai.Tai, “Dua-band microstrip bandstop filter using dual-mode loop resonator,” Electron. Lett., vol.45, no.10, May 2009
- Youngje Sung, “Dual-Mode dual-band filter with band notch structures,” Electron. Lett., vol.20, no.2, pp.73-75, Feb 2010
- Dan Cheng, Hong-Xing Zheng, Li-Ying Feng, and Feng-You Gao, “Investigation of compact second-order microstrip bandpass filter,” IEEE Microw. and Opt. Techn. Lett., vol.52, pp.1970-1973, Sept. 2010

- Erick Emmanuel Djoumessi, and Ke Wu, "Multilayer dual-mode dual-bandpass filter," *IEEE Microwave and Wireless Components Letters.*, vol.19, no.1, pp.21-23, Jan. 2009
- Wen-Hua Tu, and Kai Chang, "Piezoelectric transducer-controlled dual-mode switchable bandpass filter," *IEEE Microwave and Wireless Components Letters.*, vol.17, no.3, pp.199-201, Mar. 2007
- Wen-Hua Tu, and Kai Chang, "Miniaturized dual-mode bandpass filter with harmonic control," *IEEE Microwave and Wireless Components Letters.*, vol.17, no.12, pp.838-840, Dec. 2005
- Jung-Woo Baik, Lei Zhu, and Yong-Sik Kim, "Dual-mode dual-band bandpass filter using balun structure for single substrate configuration," *IEEE Microwave and Wireless Components Letters.*, vol.20, no.11, pp.613-615, Nov. 2010
- Falk Hettstedt, Thomas Lehmann, and Reinhard Knoechel, "Novel dual mode microstrip bandpass-filter," *IEEE Microwave Magazine.*, vol.16, Feb. 2009
- W. Kang, W. Hong, and J.Y. Zhou, "Performance improvement and size reduction of microstrip dual-mode bandpass filter," *Electron. Lett.*, vol.44, no.6, Mar. 2008

APPENDICES

APPENDIX A: Journals